A&A 585, A48 (2016)
DOI: 10.1051/0004-6361/201526396

Astronomy & Astrophysics

The Lyman continuum escape fraction of galaxies at $z = 3.3$ in the VUDS-LBC/COSMOS field⋆

A. Grazian[1], E. Giallongo[1], R. Gerbasi[2,1], F. Fiore[1], A. Fontana[1], O. Le Fèvre[3], L. Pentericci[1], E. Vanzella[4], G. Zamorani[4], P. Cassata[5], B. Garilli[6], V. Le Brun[3], D. Maccagni[6], L. A. M. Tasca[3], R. Thomas[3], E. Zucca[4], R. Amorín[1], S. Bardelli[4], L. P. Cassarà[6], M. Castellano[1], A. Cimatti[7], O. Cucciati[7,4], A. Durkalec[3], M. Giavalisco[8], N. P. Hathi[3], O. Ilbert[3], B. C. Lemaux[3], S. Paltani[9], B. Ribeiro[3], D. Schaerer[10,11], M. Scodeggio[6], V. Sommariva[7,4], M. Talia[7], L. Tresse[3], D. Vergani[6,4], A. Bonchi[1], K. Boutsia[1], P. Capak[12], S. Charlot[13], T. Contini[11], S. de la Torre[3], J. Dunlop[14], S. Fotopoulou[9], L. Guaita[1], A. Koekemoer[15], C. López-Sanjuan[16], Y. Mellier[13], E. Merlin[1], D. Paris[1], J. Pforr[3], S. Pilo[1], P. Santini[1], N. Scoville[12], Y. Taniguchi[17], and P. W. Wang[3]

(Affiliations can be found after the references)

Received 23 April 2015 / Accepted 2 August 2015

ABSTRACT

Context. The ionizing Lyman continuum flux escaping from high-redshift galaxies into the intergalactic medium is a fundamental quantity to understand the physical processes involved in the reionization epoch. However, from an observational point of view, direct detections of HI ionizing photons at high redshifts are feasible for galaxies mainly in the interval $z \sim 3$–4.

Aims. We have investigated a sample of star-forming galaxies at $z \sim 3.3$ to search for possible detections of Lyman continuum ionizing photons escaping from galaxy halos.

Methods. We used deep ultraviolet (UV) imaging in the COSMOS field, obtained with the prime focus camera LBC at the LBT telescope, along with a catalogue of spectroscopic redshifts obtained by the VIMOS Ultra Deep Survey (VUDS) to build a sample of 45 galaxies at $z \sim 3.3$ with $L > 0.5\ L^*$. We obtained deep LBC images of galaxies with spectroscopic redshifts in the interval $3.27 < z < 3.40$ both in the R- and deep U-bands (magnitude limit $U \sim 29.7$ at $S/N = 1$). At these redshifts, the R-band samples the non-ionizing 1500 Å rest-frame luminosity and the U-band samples the rest-frame spectral region just short-ward of the Lyman edge at 912 Å. Their flux ratio is related to the ionizing escape fraction after statistical removal of the absorption by the intergalactic medium along the line of sight.

Results. A subsample of ten galaxies apparently shows escape fractions >28%, but a detailed analysis of their properties reveals that, with the exception of two marginal detections ($S/N \sim 2$) in the U-band, all the other eight galaxies are most likely contaminated by the UV flux of low-redshift interlopers located close (in angular position) to the high-z targets. The average escape fraction derived from the stacking of the cleaned sample was constrained to $f_{\rm esc}^{\rm rel} < 2\%$. The implied hydrogen photoionization rate is a factor two lower than that needed to keep the intergalactic medium ionized at $z \sim 3$, as observed in the Lyman-α forest of high-z quasar spectra or by the proximity effect.

Conclusions. These results support a scenario where high redshift, relatively bright ($L \geq 0.5L^*$) star-forming galaxies alone are unable to sustain the level of ionization observed in the cosmic intergalactic medium at $z \sim 3$. Star-forming galaxies at higher redshift and at fainter luminosities ($L \ll L^*$) can only be major contributors to the reionization of the Universe if their physical properties are subject to rapid changes from $z \sim 3$ to $z \sim 6$–10. Alternatively, ionizing sources could be discovered looking for fainter sources among the active galactic nuclei population at high redshift.

Key words. galaxies: distances and redshifts – galaxies: evolution – galaxies: high-redshift – galaxies: photometry

1. Introduction

The reionization epoch marks a fundamental event in the thermal history of the Universe, probably located in the redshift interval $z = 6$–10. The lower limit is derived from observations of the Gunn-Peterson effect in $z = 6$ quasar spectra (Fan et al. 2006), while the upper end comes from measurements of the Thomson scattering in the cosmic microwave background (CMB) polarization map by *Wilkinson* Microwave Anisotropy Probe (WMAP; Hinshaw et al. 2013) and *Planck* (Planck Collaboration XIII 2015). The time extension of the reionization processes can also be constrained by the so-called kinetic Sunyaev-Zel'dovich (kSZ) effect. Combining data from the South Pole Telescope (SPT) with the WMAP results, Zahn et al. (2012) provided a 95% c.l. limit to the duration of reionization of $\Delta z \leq 4.4$ and placed the end of reionization at $z = 7.2$. While we are able to approximately locate the reionization epoch, we still do not have a clear perception of the sources providing the bulk of the ultraviolet (UV) photons required to reionize the Universe. Prime suspects have been searched so far among high-redshift, star-forming galaxies or active galactic nuclei (AGNs).

It is well known that bright quasars (QSOs) are efficient producers of HI ionizing photons ($\lambda \leq 912$ Å), and they can ionize large bubbles of hydrogen and helium even at distances up to several Mpcs (Cowie et al. 2009; Prochaska et al. 2009; Worseck et al. 2014a; Stevans et al. 2014). However, their volume density is apparently too low at high redshifts ($z > 2$) to

⋆ Based on data obtained with the European Southern Observatory Very Large Telescope, Paranal, Chile, under Large Programme 185.A-0791 and on observations made at the Large Binocular Telescope (LBT) at Mt. Graham (Arizona, USA).

provide the cosmic photoionization rate required to keep the intergalactic medium (IGM) ionized at $z \sim 6$ (Fan et al. 2006). Recent searches for low luminosity AGNs at high redshifts by means of deep X-ray imaging are gradually changing this scenario (Fiore et al. 2012; Giallongo et al. 2012, 2015), leaving room for important contributions to the reionization by this fainter AGN population.

High-redshift, star-forming galaxies can also be important contributors of ionizing photons at $z \geq 2$ (Haardt & Madau 2012; Duncan & Conselice 2015). An intense star formation activity is observed up to $z \sim 8-10$ (see for example McLeod et al. 2015), and the luminosity function (LF) of galaxies at $z \geq 4$ is gradually steepening with redshift (Finkelstein et al. 2015; Bouwens et al. 2015a). Young stellar populations inside high-redshift galaxies are producing a large amount of UV photons, but only a fraction of them can reach the surrounding IGM. An efficient way of parametrizing the emission of HI ionizing photons, w.r.t. the non-ionizing photons, is the definition of the escape fraction (Steidel et al. 2001). The escape fraction parameter is a measurement of the fraction of HI ionizing photons, which are not absorbed by the interstellar medium (ISM) and are thus free to ionize the neutral hydrogen in the IGM. The extensive definition of the escape fraction is provided in Sect. 3.

In general, bright star-forming galaxies at low redshifts ($z \leq 2$) are not able to ionize their neighbourhoods since their escape fractions are only few percents or less (Grimes et al. 2009; Cowie et al. 2009; Siana et al. 2010; Bridge et al. 2010; Leitet et al. 2013). At high redshifts, the current situation is not so clear. The escape fractions from $z \geq 3$ star-forming galaxies measured by different groups in the last 15 yr led to different results, indicating that some systematics are still present in the analysis and in the galaxy samples used.

Steidel et al. 2001 claimed the detection of significant emission ($f_{\rm esc}^{\rm rel} \sim 50\%$) of Lyman continuum (LyC) photons from the composite spectrum of 29 Lyman break galaxies (LBG) at $z \sim 3$. Two LBGs from the Steidel high-redshift sample were spectroscopically observed at intermediate resolution by Giallongo et al. (2002) with very deep integration. They only derived an upper limit to the relative escape fraction of $f_{\rm esc}^{\rm rel} \leq 16\%$. Further spectroscopic work by Steidel's team found only two emitting galaxies at $z \sim 3$, out of 14 analysed, with a significant escape fraction ($f_{\rm esc}^{\rm rel} \geq 50-100\%$). For the remaining population, only upper limits were derived resulting in an average $f_{\rm esc}^{\rm rel} \sim 14\%$ for the whole sample (Shapley et al. 2006). However, the two emitting galaxies were not confirmed as LyC emitters by Iwata et al. (2009) and Nestor et al. (2011). The original result of Shapley et al. (2006) should thus be converted into a strict upper limit of $f_{\rm esc}^{\rm rel} \leq 2\%$ at $z \sim 3$ (Cooke et al. 2014).

With the aid of narrowband imaging at $\lambda \sim 3590$ Å, Iwata et al. (2009) and Nestor et al. (2011) studied the same area of Shapley et al. (2006), namely the SSA22 field. They found a significant population of LyC emitters at $z \geq 3$, with escape fractions in the range $f_{\rm esc}^{\rm rel} \sim 4-100\%$ (some Lyman-α emitters with $f_{\rm esc}^{\rm rel} \geq 100\%$), providing the first indication that the escape fraction of galaxies started to increase at $z \geq 3$ (or that their sample may be contaminated by foreground objects, as we discuss in the following). Recently, Mostardi et al. (2013) studied a new sky region around an overdensity of sources at $z \sim 2.8$, reaching slightly similar conclusions ($f_{\rm esc}^{\rm rel} \sim 5-49\%$).

Results from other teams based on very deep narrow- or broadband UV imaging gave only stringent upper limits of $f_{\rm esc}^{\rm rel} \leq 5-10\%$ to the escape fraction of star-forming galaxies at $z = 3-4$ (Vanzella et al. 2010b; Boutsia et al. 2011). The main reason for the discrepant results is due to the details of the photometric analysis and to the different morphological analysis of the candidate LyC emitters.

The most convincing explanation for this discrepancy has been proposed by Vanzella et al. (2010a) on the basis of possible UV flux contamination in the Nestor's and Mostardi's LyC emitting sample by low-redshift interlopers, which are near the position of the high-redshift galaxies. As estimated by Vanzella et al. (2010a), the chance for contamination increases with large seeing and deep UV images. Considering a sample of 101 galaxies at $3.4 \leq z \leq 4.4$ in the Great Observatories Origins Deep Survey southern (GOODS-South) field, they only found one convincing detection after removing probable contaminants identified on the basis of accurate multi-colour HST photometry at high angular resolution.

At the same time, Boutsia et al. (2011) studied a small sample of eleven galaxies at $z \sim 3.3$ in the Q0933, Q1623, and COSMOS fields with very deep imaging in the U- and R-bands obtained at the prime focus camera LBC of LBT. The non-detection of all the galaxies resulted in a strict upper limit to the escape fraction of $f_{\rm esc}^{\rm rel} < 5\%$, but the result was affected by low number statistics and by the uncertainty due to the stochasticity of the IGM absorption. Their conclusions were that, at present, a class of ionizing sources responsible for cosmic reionization has not been clearly identified and a step forward to the escape fraction studies is required.

Recently, Siana et al. (2015) reanalysed, with the HST instrument WFC3-UVIS, five galaxies that were identified by Nestor et al. (2011) as LyC candidates at $z \sim 3.1$. Thanks to deep *F336W* images and near infrared (NIR) Keck spectra of these galaxies, Siana et al. (2015) concluded that the supposed LyC emission is in fact provided by lower redshift interlopers. The new upper limit by these observations is $f_{\rm esc}^{\rm rel} \sim 7-9\%$, consistent with the limits by Vanzella et al. (2010b) and Boutsia et al. (2011). In addition, Mostardi et al. (2015) reported an HST follow-up analysis of 16 candidate LyC emitters found by Mostardi et al. (2013). These authors obtained deep U_{336}, V_{606}, J_{125}, and H_{160} imaging with WFC3 and ACS for these galaxies: thanks to the high spatial resolution of HST, they showed that 15 emitters can be explained by contamination of low-z objects, wrong spectroscopic redshifts, or uncertain photometric redshifts. Only one galaxy shows a robust LyC detection, according to Mostardi et al. (2015). On the basis of these results, they concluded that galaxies at $z \sim 3$ provide the same contribution of QSOs to the HI photoionizing background, although with large uncertainties.

Increasing the number of accurate LyC measures is not a trivial task since it requires either very deep spectroscopy or very deep UV imaging of a large sample of galaxies with known spectroscopic redshifts in the range $z = 3-4$, where the IGM still allows the transmission of some ionizing flux along the line of sight (Inoue et al. 2014). Indeed, at higher redshifts it is difficult to disentangle the absorption due to the galaxy ISM from that due to the surrounding IGM along the line of sight (LoS).

In this work, we exploit the availability of very deep U-band photometry obtained with the LBC prime focus imager at LBT, coupled with a large number of galaxies with spectroscopic redshifts in a relatively narrow range around $z \simeq 3.3$, which allows the UV band to sample the spectral region just shortward of 912 Å rest. The spectroscopic sample is taken from the VIMOS Ultra Deep Survey (VUDS, Le Fèvre et al. 2015) of high-redshift galaxies ($2 < z < \sim 6$) in the COSMOS field where deep HST imaging is also available and allows us to look for possible contamination by low-redshift interlopers.

This paper is organized as follows. In Sect. 2 we present the data set, in Sect. 3 we describe the method adopted, in Sects. 4 and 5 we show the results for individual objects and for the overall sample as a whole, in Sect. 6 we discuss our results, and in Sect. 7 we provide a summary. Throughout the paper we adopt the Λ cold dark matter (Λ-CDM) concordance cosmological model ($H_0 = 70$ km s^{-1} Mpc^{-1}, $\Omega_M = 0.3$ and $\Omega_\Lambda = 0.7$). All magnitudes are in the AB system.

2. Data

We selected the COSMOS field (Scoville et al. 2007) as an optimal area for the measurement of the escape fraction of galaxies at $z \sim 3$, given its combination of deep multi-wavelength imaging by LBC coupled with a large number of spectroscopic surveys over a broad redshift interval $0 < z < 7$ obtained by extensive observational campaigns (Lilly et al. 2007; Le Fèvre et al. 2015).

In the present analysis, we also included the galaxies already studied by Boutsia et al. (2011) in the Q0933 and Q1623 fields.

2.1. The photometric data set

The imaging data set used in this paper consists of deep LBC observations of the COSMOS field in the U and R filters. These deep observations are part of a more ambitious programme, the LBC/Cosmic Assembly Near-infrared Deep Extragalactic Legacy Survey (LBC/CANDELS, Grazian et al., in prep.) survey, with the goal of providing complementary deep UV coverage with LBC to the northern fields (COSMOS, GOODS-North, EGS) of the CANDELS survey (Grogin et al. 2011; Koekemoer et al. 2011). The LBC imaging data set of the COSMOS field has been described in detail in Boutsia et al. (2011) and Boutsia et al. (2014).

The LBC instrument (Giallongo et al. 2008) has two wide-field imagers, one optimized for the UV wavelengths and the other for the optical red bands. This imager has observed part (~0.20 sq. deg) of the COSMOS (Scoville et al. 2007) field in *UGRIZ*-bands to search for LBGs at $2.7 < z < 3.4$ (Boutsia et al. 2014). We obtained these data at the LBT with LBC, one of the most efficient ground-based, large-field UV imager's at an 8-meter class telescope, which has allowed us to derive a stringent limit of ≤5% to the escape fraction of eleven star-forming galaxies at $z \sim 3.3$ (Boutsia et al. 2011), using the same technique that is adopted in this work.

The U-band observations of the COSMOS field by LBC are constituted of three partially overlapping pointings of ~6 h each, for a total of 11 h of exposure on the deepest regions. The relative good seeing (~1.0 arcsec) and the high sensitivity of the LBC camera in the UV allow us to reach a depth of 28.7 AB magnitudes (at $S/N = 1$) over an area corresponding to 700 sq. arcmin., with slightly deeper limits (~29.1) on the regions covered twice (~450 sq. arcmin).

The R-band data set has an average seeing of 0.9 arcsec and in 3.3 h of exposure time it reaches, for two-thirds of the area covered by deep U-band imaging, a depth of $R = 25.7$ AB magnitude at $S/N = 10$. The third pointing is shallower ($R = 23.8$), since the exposure time was shorter (450 s). In this subregion, we select only galaxies down to $R \leq 24.0$ to work at a good S/N in the detection band, which is used to measure the non-ionizing continuum of the sources.

The standard LBC pipeline has been used to reduce the imaging data set, as described in detail in Giallongo et al. (2008), Boutsia et al. (2011, 2014). In particular, after correcting the images for bias subtraction, we applied standard flat-fielding using sky flats obtained during twilight. The sky background was estimated using SExtractor (Bertin & Arnouts 1996) with a mesh of 64 by 64 pixels and adopting a median of 3 by 3 meshes. The astrometric corrections were computed using the software "AstromC" described by Radovich et al. (2004). After resampling all the individual images in a common reference frame, we co-added the various images to create deep mosaics for each field.

For each LBC image, we derived a careful estimate of the absolute rms map taking the Poisson statistics and the instrumental gain for each individual chip into account, as described in Boutsia et al. (2011). We then propagated the rms map over the whole data reduction chain, obtaining an absolute variance map associated with each stacked scientific frame as a final product of the pipeline.

2.2. Spectroscopic redshifts

The VUDS spectroscopic survey (Le Fèvre et al. 2015) is an ESO Large Programme (P.I. Le Fèvre) with the aim of obtaining ~10 000 spectroscopic redshifts with the VIMOS instrument to study early phases of galaxy evolution in the redshift range $2 < z < 6$ and beyond. This ambitious programme has been conducted over three fields (VVDS-02h, COSMOS, ECDFS) and the targets were selected with different criteria (inclusive combination of U-dropout, B-dropout, and photometric redshift selections), tailored to maximize the efficiency of finding galaxies at $3 < z < 5$, and thus is complementary to the zCOSMOS survey (Lilly et al. 2007). The spectra are the result of deep integration (14 h per target) covering the wavelength range $3650 \leq \lambda \leq 9350$ Å. Details about the observational strategy, candidate selection, data reduction, quality flag assignment, and first results of the VUDS survey can be found in Le Fèvre et al. (2015). The data acquisition, reduction, and redshift extraction procedure of the whole VUDS survey have recently been completed.

We focus on a very small redshift range ($3.27 < z < 3.40$) to minimize the effect of the strong IGM opacity evolution with redshift (Inoue et al. 2014; Worseck et al. 2014a) and to facilitate a direct measurement of the relative ionizing escape fraction from star-forming galaxies at $z = 3.3$. As explained also in Boutsia et al. (2011), this narrow redshift range allows us to use the LBC U-band filter (SDT-Uspec) to sample the rest-frame wavelengths short-ward of, but not too far from, 912 Å, namely at ≥880 Å rest frame. An extension of the redshift range at $z > 3.40$ is possible, but it requires detail simulations of the variance due to the stochasticity of intervening damped Lyman-α systems (DLAs) or Lyman Limit systems (LLs), as shown in Vanzella et al. (2010b). Since it goes beyond the scope of this paper, we limit the analysis to $z < 3.40$.

We started from the sample of 73 galaxies with highly reliable (flag = 3, 4, 23, 24) spectroscopic redshifts within the interval $3.27 < z < 3.40$ in the COSMOS area covered by the VUDS spectroscopic survey. We do not consider within our sample the AGNs from the optical classification of the VUDS spectra (flag = 11, 12, 13, 14, 19 or 211, 212, 213, 214, 219 due mainly to the presence of a strong CIV emission line). We excluded also the spectroscopic redshifts based only on a single emission line (flag = 9 or 29). Of the pure (non AGN) galaxies, only 35 are covered by the LBC images in the U- and R-bands, which do not cover the whole COSMOS field, as

Table 1. Galaxies in the VUDS-LBC/COSMOS field used to derive the LyC relative escape fraction.

ID_{LBC}	Field	RAD (deg)	Dec (deg)	z_{spec}	R mag (AB)	U mag (AB)	M_{1500}	f_{esc}^{rel}	Cont
13903	COSMOS	150.414993286	+2.159081936	3.290	22.59	≥28.69	–23.11	≤ 0.039	No
74113	COSMOS	149.886260986	+2.276002169	3.330	23.56	≥29.50	–22.14	≤ 0.045	No
56982	COSMOS	149.847152710	+2.373027802	3.356	23.65	≥29.46	–22.05	≤ 0.051	No
72509	COSMOS	149.994003296	+2.285038948	3.374	23.84	≥29.38	–21.86	≤ 0.065	No
16700	COSMOS	149.940277100	+2.082487583	3.354	24.44	≥29.83	–21.26	≤ 0.075	No
61293	COSMOS	149.870300293	+2.349019766	3.292	23.90	≥29.13	–21.80	≤ 0.087	No
21413	COSMOS	149.974533081	+2.111910582	3.319	24.50	≥29.68	–21.20	≤ 0.091	No
31070	COSMOS	149.912933350	+2.236840248	3.333	24.74	≥29.86	–20.96	≤ 0.096	No
64371	COSMOS	150.051940918	+2.332614422	3.370	24.19	≥29.26	–21.51	≤ 0.100	No
49197	COSMOS	149.978881836	+2.135632515	3.395	24.81	≥29.80	–20.89	≤ 0.108	No
58808	COSMOS	149.962997437	+2.363846302	3.359	24.63	≥29.58	–21.07	≤ 0.112	No
68731	COSMOS	150.138900757	+2.307063818	3.288	24.47	≥29.41	–21.23	≤ 0.113	No
32388	COSMOS	149.778930664	+2.229439735	3.300	24.63	≥29.53	–21.07	≤ 0.118	No
16446	COSMOS	149.961273193	+2.081201315	3.270	24.96	≥29.86	–20.74	≤ 0.118	No
69814	COSMOS	149.834243774	+2.300836325	3.366	24.56	≥29.45	–21.14	≤ 0.119	No
3400	Q0933	143.354507446	+28.806911469	3.270	24.88	≥29.76	–20.82	≤ 0.120	No
1723	COSMOS	150.447082520	+2.347564697	3.300	23.63	≥28.43	–22.07	≤ 0.129	No
56248	COSMOS	149.917510986	+2.378670692	3.288	24.71	≥29.50	–20.99	≤ 0.130	No
63275	COSMOS	149.983078003	+2.338610888	3.343	24.96	≥29.72	–20.74	≤ 0.134	No
72124	COSMOS	149.883422852	+2.286791325	3.352	24.71	≥29.46	–20.99	≤ 0.135	No
51227	COSMOS	149.892135620	+2.414754868	3.280	24.45	≥29.18	–21.25	≤ 0.137	No
50989	COSMOS	149.834274292	+2.416670561	3.310	24.61	≥29.32	–21.09	≤ 0.140	No
51473	COSMOS	150.065383911	+2.411855936	3.355	25.29	≥29.90	–20.41	≤ 0.153	No
8556	Q0933	143.382461548	+28.753007889	3.330	24.91	≥29.51	–20.79	≤ 0.155	No
17175	Q1623	246.469177246	+26.892374039	3.340	24.69	≥29.29	–21.01	≤ 0.155	No
47539	COSMOS	149.888641357	+2.144912004	3.311	25.02	≥29.59	–20.68	≤ 0.159	No
30576	COSMOS	150.141159058	+2.239602089	3.336	25.26	≥29.82	–20.44	≤ 0.160	No
10235	COSMOS	150.106704712	+2.044517517	3.328	25.14	≥29.70	–20.56	≤ 0.161	No
70238	COSMOS	149.853439331	+2.298267603	3.292	24.58	≥29.13	–21.12	≤ 0.162	No
42374	COSMOS	150.137237549	+2.174738884	3.294	25.44	≥29.87	–20.26	≤ 0.181	No
19739	COSMOS	149.934432983	+2.102468014	3.316	25.54	≥29.96	–20.16	≤ 0.183	No
12646	Q0933	143.328750610	+28.719076157	3.330	25.13	≥29.50	–20.57	≤ 0.192	No
10849	Q0933	143.360122681	+28.734085083	3.350	25.59	≥29.92	–20.11	≤ 0.198	No
65540	COSMOS	149.848281860	+2.325203896	3.320	25.50	≥29.58	–20.20	≤ 0.250	No
4890	COSMOS	149.824325562	+2.009310722	3.301	25.24	≥29.24	–20.46	≤ 0.268	No
19521	COSMOS	150.330398560	+2.072281122	3.303	22.55	26.50	–23.15	0.281[a]	Yes
63327	COSMOS	149.843582153	+2.340100288	3.329	25.02	28.47	–20.68	0.446[b]	No
25155	COSMOS	149.857284546	+2.270117283	3.364	25.24	28.61	–20.46	0.479[c]	No
40998	COSMOS	149.952316284	+2.182848215	3.321	25.19	28.36	–20.51	0.577[d]	Yes
48734	COSMOS	149.815368652	+2.138106108	3.384	24.99	27.99	–20.71	0.674[e]	Yes
47357	COSMOS	150.096496582	+2.145905495	3.292	24.91	27.78	–20.79	0.760[f]	Yes
52336	COSMOS	149.980270386	+2.405712605	3.371	24.85	27.06	–20.85	1.400	Yes
55594	COSMOS	149.939086914	+2.388362885	3.334	24.17	26.06	–21.53	1.873	Yes
16669	COSMOS	149.994964600	+2.080330372	3.367	24.39	26.06	–21.31	2.295	Yes
72687	COSMOS	149.877334595	+2.283946991	3.328	24.14	25.55	–21.56	2.920	Yes

Notes. The galaxies have been sorted in ascending order of relative escape fraction. The *upper part* of the table summarizes the non-detections (i.e. $S/N < 1$) in the LBC U-band, for which an upper limit to the relative escape fraction has been provided. The central subsample includes galaxies with apparent LyC detection, while the last four galaxies have escape fraction larger than 1.0 (i.e. 100%) and are thus considered unreliable, probably as a result of foreground contamination, as discussed in the main text. The last column, labelled Cont, indicates whether a galaxy is possibly contaminated by foreground emission. Notes on individual objects: [(a)] local escape fraction 1.75, calculated on the LyC emission region only; [(b,c)] they can be plausible LyC emitters; [(d)] local escape fraction 4.51; [(e)] local escape fraction 6.40; [(f)] local escape fraction 5.13.

mentioned above. One of these sources has been excluded since it falls on an horizontal stripe of bad pixels caused by a saturated star in the LBC images. Eleven additional galaxies were already discussed by Boutsia et al. (2011), resulting in a total sample of 45 star-forming galaxies at $z \sim 3.3$ with secure spectroscopic redshifts and deep U- and R-band images by LBC. Table 1 summarizes the properties of the individual galaxies, which we use to study the escape fraction at $z = 3.3$.

3. The adopted method to derive the LyC escape fraction of star-forming galaxies in the VUDS-LBC/COSMOS field

We exploit the deep UV imaging by LBC in the VUDS/COSMOS field to derive a meaningful measurement of the ionizing radiation of star-forming galaxies at $z \sim 3.3$.

The LyC escape fraction of high-z galaxies can be evaluated by adopting very deep UV imaging data sampling the $\lambda \leq 912$ Å rest-frame region. Since the intrinsic spectral energy distribution (SED) of a galaxy is not known a priori, especially in the rest-frame far UV where significant dust reddening could be present, a relative escape fraction is usually derived from the observations (Steidel et al. 2001). It is defined as the fraction of escaping LyC photons divided by the fraction of escaping photons at 1500 Å rest frame (Siana et al. 2007).

The SED of a high-redshift source at $\lambda \leq 912$ Å rest frame is also affected by the photoelectric absorption by the IGM (Moller & Jakobsen 1990; Madau 1995) and it is mainly due to LLs with column densities of neutral hydrogen between $\log(N_{\rm HI}) \sim 17$ and 20. We adopt the recent estimates by Worseck et al. (2014a) to correct for the mean effect of the IGM absorption. We obtain an IGM mean transmission $\langle \exp(-\tau_{900}^{\rm IGM}) \rangle = 0.28$ at $z \sim 3.3$, which is similar to that found adopting the IGM corrections by Prochaska et al. (2009), by convolving the IGM absorption at $z = 3.3$ with the U-band filter of LBC and adopting the same procedure outlined in Boutsia et al. (2011).

It is worth noting that we are not considering the variance of the IGM absorption in different LoS due to a patchy pattern of LLs. Our relatively large number of galaxies allows us to deal, from the statistical point of view, with the possibility that few LoS are completely absorbed by intervening optically thick systems at $z \leq 3.3$. In the discussion section, we quantify this probability.

Following Steidel et al. (2001) and Siana et al. (2007), we estimate the relative escape fraction using the following equation:

$$f_{\rm esc}^{\rm rel} = \frac{(L_{1500}/L_{900})_{\rm int}}{(F_R/F_U)_{\rm obs}} \exp\left(\tau_{900}^{\rm IGM}\right), \quad (1)$$

which is equivalent to

$$f_{\rm esc}^{\rm rel} = \exp(-\tau_{\rm HI}) \times 10^{-0.4(A_{900}-A_{1500})} = f_{\rm esc}^{\rm abs} \times 10^{0.4A_{1500}}, \quad (2)$$

where $(L_{1500}/L_{900})_{\rm int}$ is the ratio of the intrinsic luminosities at 1500 and 900 Å rest frame, $(F_R/F_U)_{\rm obs}$ is the ratio of the observed fluxes in the R- and U-band, $\exp(-\tau_{\rm HI})$ indicates the ISM extinction, $\exp(-\tau_{\rm HI}) \times 10^{-0.4A_{900}}$ is the absolute escape fraction $f_{\rm esc}^{\rm abs}$, A_{1500}, and A_{900} are the dust absorption coefficients at 1500 and 900 Å, respectively. According to Calzetti et al. (2000), $A_{1500} = 10.33E(B-V)$ and $A_{900} = 18.02E(B-V)$, thus giving $f_{\rm esc}^{\rm rel} = 2.59 f_{\rm esc}^{\rm abs}$ for $E(B-V) = 0.1$. According to Eq. (2), this implies that $f_{\rm esc}^{\rm rel}$ is always less than 100%.

We adopt an intrinsic ratio of $(L_{1500}/L_{900})_{\rm int} = 3$ for our star-forming galaxies, taking the absorption produced by the stellar atmospheres into account, as adopted by Steidel et al. (2001) and Boutsia et al. (2011) on the basis of predictions by the spectral synthesis stellar models. The intrinsic ratio $(L_{1500}/L_{900})_{\rm int}$ depends on the physical properties of the galaxies, mainly the mean stellar ages, metallicities, initial mass functions (IMFs), and star formation histories (SFHs). For typical star-forming galaxies, at $z \sim 3.3$ the intrinsic ratio $(L_{1500}/L_{900})_{\rm int}$ varies between 1.7 and 7.1 for an age between 1 Myr and 0.2 Gyr, adopting the Bruzual & Charlot (2003) library (BC03). In the following sections, we discuss the implications of our choice, and we show that our final results on the ionization emissivity are robust against the adopted value of 3 for the intrinsic ratio $(L_{1500}/L_{900})_{\rm int}$. To derive the observed fluxes at 900 and 1500 Å rest frame at $z \sim 3.3$, we rely on the U- and R-band flux ratio measured by LBC, $(F_R/F_U)_{\rm obs}$.

In our previous paper (Boutsia et al. 2011), we estimated fluxes using aperture photometry matched to the seeing of the U- and R-bands. Here we explore a slightly different approach: if LyC photons are emitted by a particular region of a galaxy characterized by low ISM absorption, then we must also observe non-ionizing emission emerging from the same spatial region (see Sect. 4.1.1 of Vanzella et al. 2012a). As a consequence, the emission in the U-band (sampling ~900 Å at $z \sim 3.3$) must be always associated with an emission in the R-band (~1500 Å at $z \sim 3.3$). The opposite would not be true, however, since non-ionizing radiation can be detected in regions of a galaxy where the ISM or dust absorption are elevated, with a negligible emission of LyC photons. The observed profile of a galaxy in the R-band can thus only be used to measure the ionizing radiations in the U-band in the physical regions where such photons are expected. This limits the contamination by foreground galaxies that by chance lie on a given LoS of a star-forming galaxy at $z \sim 3.3$. We thus adopt the ConvPhot software (De Santis et al. 2007) to derive less contaminated photometry in the U-band, using the R-band image, with its much higher S/N, as a prior to reconstruct the profile of galaxies in the U-band. Although the computed magnitude is not significantly different from that derived by aperture photometry, the photometric uncertainties are smaller in the ConvPhot procedures since the flux errors in the U-band are, at least at a first approximation, equal to the result of the sum over its rms^2 weighting for the profile of the object in the R-band. Comparing the objects in common with Boutsia et al. (2011), we find that this new method enables a gain by a factor of ~1.7 in S/N in the U-band photometry, and thus a similar improvement on the determination of the uncertainties in the LyC escape fraction. The resulting limiting magnitude in the LBC U-band image is thus ~29.7 AB at $S/N = 1$ for the central overlapping region, and slightly shallower (~29.3) in the flanking areas only covered with one LBC pointing.

Following Vanzella et al. (2012a), we define the "local" escape fraction as the parameter measuring the LyC emission, w.r.t. non-ionizing radiation, measured in the same physical region where both the 900 and 1500 Å rest-frame wavelengths are emitted. As a sanity check for the consistency of the following results, the "local" escape fraction cannot exceed 100% for reasonable values of the IGM transmission and of the intrinsic ratio $(L_{1500}/L_{900})_{\rm int}$. As in Vanzella et al. (2012a), a "local" escape fraction of 500–1000% can be a clear indication of contamination in the LyC band from a foreground interloper.

4. The relative escape fraction of individual galaxies at $z \sim 3.3$

Using the method outlined in the previous section, we computed the relative escape fraction of the 45 individual galaxies at $3.27 \leq z_{\rm spec} \leq 3.40$ of the VUDS-LBC/COSMOS sample. In case of a non-detection in the U-band (i.e. $S/N < 1$), we provide the upper limit of the relative escape fraction at 1σ. This is a fair limit since we are forcing the measurement of LyC flux in a region where we see radiation at $\lambda \sim 1500$ Å rest frame (non-ionizing) from the clear detection in the R-band. Table 1 summarizes the properties of these objects. As we discuss in Sect. 6.2,

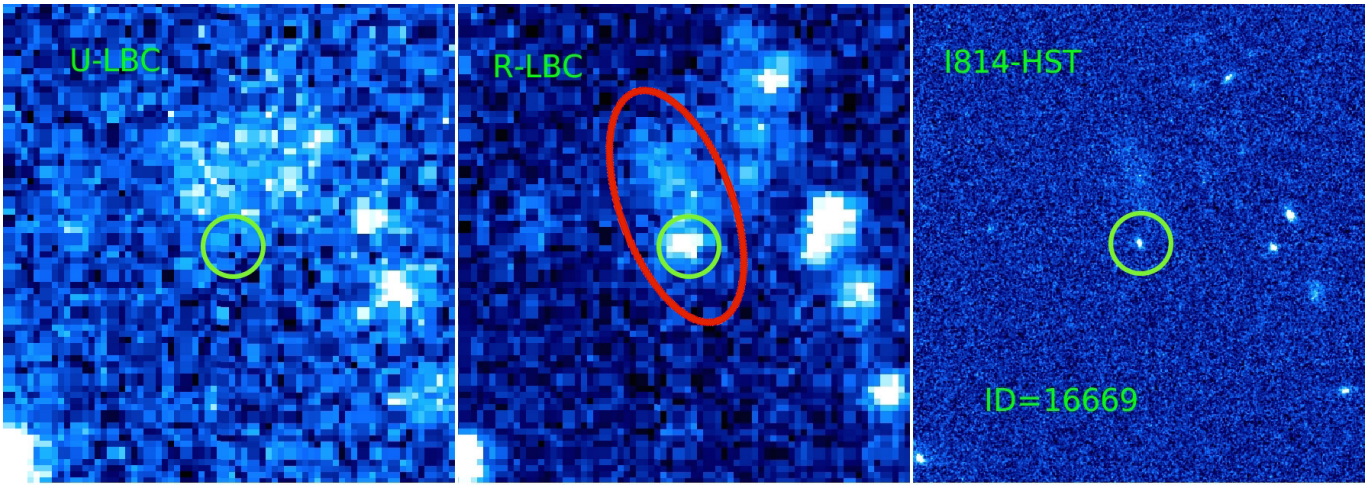

Fig. 1. Cutouts of source ID = 16669 in the U-band (*left*) and in the R-band (*centre*) by the LBC instrument. The cutout on the *right* shows the same sky area observed by HST in the *I814W* filter. The position of the galaxy with spectroscopic redshift is indicated with a green circle. A diffuse emission at the north of the $z \sim 3.3$ galaxy is detected in all the three bands. The red ellipse in the central panel indicates the area covered by source ID = 16669 in the LBC R-band. This region has been used to compute the global escape fraction provided in the last column of Table 1. The size of each image is 20 arcsec by 20 arcsec.

the patchy nature of the IGM makes the determination of the escape fraction for individual galaxies slightly uncertain. Our main results have thus been derived in Sect. 5.1 by studying the properties of the whole galaxy population at $z \sim 3$ through image stacking.

Table 1 shows that there are ten detections in the U-band, within the initial sample of 45 star-forming galaxies at $z \sim 3.3$ in the VUDS area, covered by LBC observations (complemented with early results from Boutsia et al. 2011). At face value, this result suggests possible LyC emission for this subsample.

4.1. Galaxies with possible LyC detection

We discuss here the properties of the ten interesting objects at $z \sim 3.3$, which are detected in the U-band of LBC showing possible ionizing emission. In the next subsections, we check the reliability of the LyC sources based on the deep HST *F814W* (hereafter indicated as *I814W*) band and the LBC U- and R-bands.

4.1.1. Galaxies with $f_{\rm esc}^{\rm rel} > 100\%$

In Table 1 there are four galaxies with a non-physical escape fraction, ranging between 140 and 292% (last four objects at the end of the table).

As an example of escape fraction exceeding 100%, Fig. 1 shows the cutouts in the LBC U- and R-bands, as well as the HST image in the *I814W* filter, of the galaxy with ID = 16669 listed in Table 1. The spectroscopic redshift from VUDS is associated with a compact galaxy (indicated with the green circle in the HST image on the right). The compact source falls near (distance = 2.1 arcsec) a bright and extended object, which is clearly detected in the U-band, while at the position of the $z \sim 3.3$ galaxy no flux is emitted in the U-band. When computing the escape fraction with our method (i.e. detecting the galaxy in the LBC R-band and measuring the LyC flux in the LBC U-band on the same area, shown by the red ellipse in the central panel of Fig. 1), the two galaxies are merged in a single detection in the R-band, and thus our procedure gives a significant LyC detection from the U-band. Translating the observed U- and R fluxes into an escape fraction, it turns out that this object has $f_{\rm esc}^{\rm rel} = 229.5\%$, more than twice the maximum value allowed for a typical star-forming galaxy. If we restrict the investigated area to the region with a significant U-band emission (the area of the red ellipse in Fig. 1 outside the green circle; this barely extended object is also visible in the HST image), and we compute the flux ratio between the U- and R-band, we end up with an escape fraction of 519.4%. The uncertainties in the U- and R magnitudes are on the order of ~0.05, indicating that the latter estimate of the local escape fraction is robust. The extended galaxy on top of the compact $z \sim 3.3$ source is 3 arcsec in diameter, which corresponds to 22 kpc if the two galaxies are at the same redshift, while Bouwens et al. (2004) found that a typical $L*$ star-forming galaxy has a half-light radius of 2 kpc at $z \sim 2.5$. A plausible explanation for the detection in LyC for source ID = 16669 is thus the presence of a foreground object, which mimics the presence of a LyC region near the $z \sim 3.3$ galaxy.

A similar situation happens for sources ID = 52336 and 55594 (Fig. A.1), where the presence of an extended galaxy and a compact object, respectively, with relatively bright U-band emission and significant offset (distance of 2.4 and 1.5 arcsec, respectively) from the $z \sim 3.3$ objects (green circles) clearly indicates the superposition of foreground sources. The global escape fractions for these two galaxies are 140% and 187%, respectively. If we compute instead the local escape fraction only from the region with clear detection in the U-band, we end up with even larger escape fractions of 966% and 654%, respectively. Even in this case the most plausible explanation is a contamination by a foreground galaxy prospectively close to the $z \sim 3.3$ source.

The situation is less clear for source ID = 72687 in Table 1. This galaxy has an escape fraction of 292%, which is clearly not physical under reasonable assumptions for the stellar populations involved and for the IGM absorption. From an analysis of the HST image (Fig. 2), we cannot confirm with high confidence the presence of two different objects as in the previous cases, although two distinct blobs are seen in the HST thumbnail. From a detailed analysis of the LBC images, we find a small shift of ~0.5 pixel, corresponding to ~0.1 arcsec, from the centre of the source in the R-band and in the U-band. The separation between the two blobs in the HST image is slightly

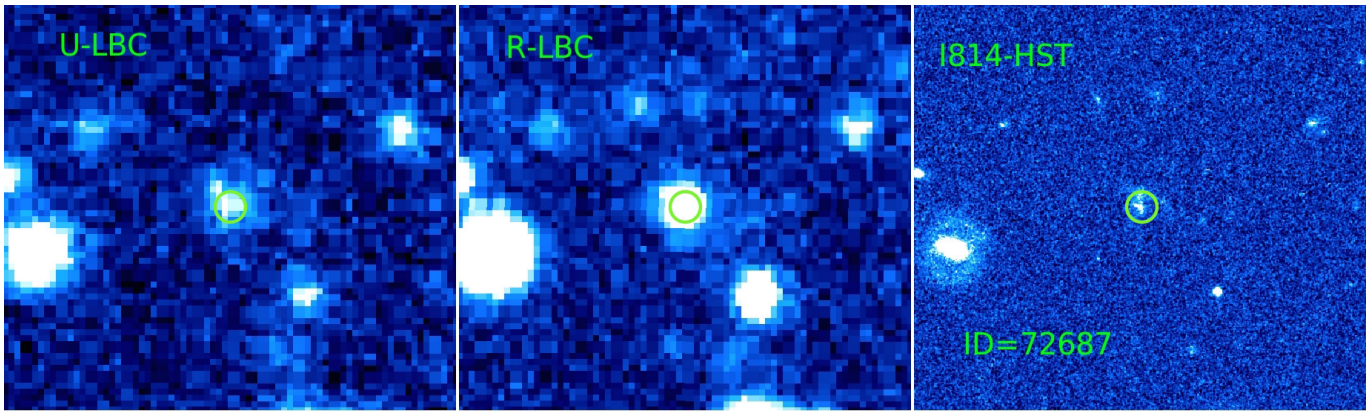

Fig. 2. Cutouts of source ID = 72687 in the *U*-band (*left*) and in the *R*-band (*central panel*) by the LBC instrument. The *right* cutout shows the same sky area observed by HST in the *I814W* filter. The position of the spectroscopic redshift is indicated with a green circle. The size of each image is 14 arcsec by 14 arcsec. In this case, the presence of two distinct objects is not secure, despite the availability of the HST image, but there is some hint of the presence of two blended galaxies in the latter. The object in the *U*-band is slightly offset (~0.1 arcsec) from the centre of the source detected in the LBC *R* and HST *I814W* bands.

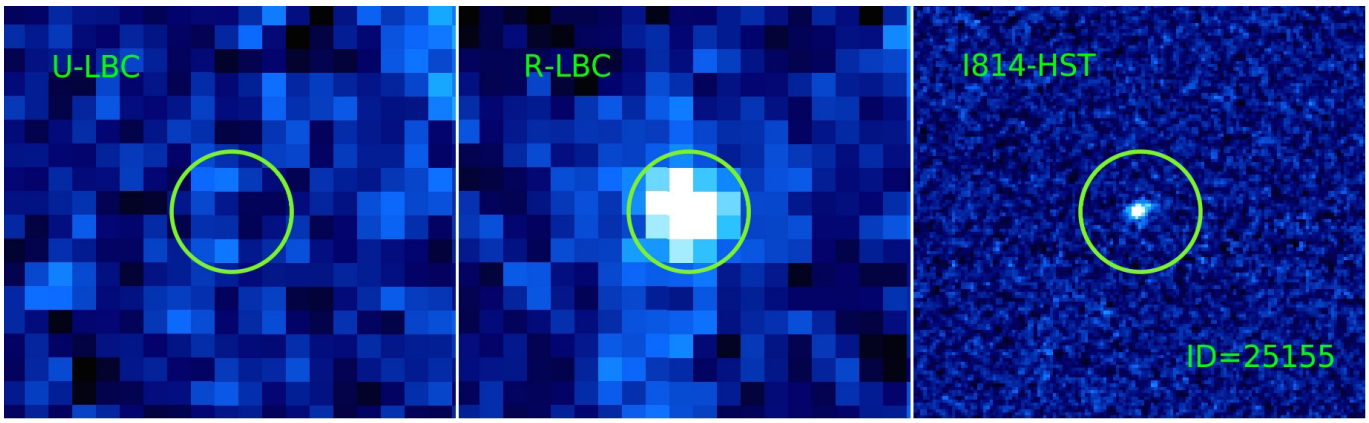

Fig. 3. Cutouts of source ID = 25155 in the *U*-band (*left*) and in the *R*-band (*centre*) by the LBC instrument. The cutout on the *right* shows the same sky area observed by HST in the *I814W* filter. The position of the spectroscopic redshift is indicated with a green circle. The size of the cutouts is 4.3 arcsec. This object seems isolated in the HST *I814W* band, but there is a possible hint of the presence of a very faint source in the north-west of the bright galaxy at $z \sim 3.3$. There is a detection at $\sim 2\sigma$ level in the *U*-band of LBC.

larger, of 0.3 arcsec. This could be an other case of blending of a $z \sim 3.3$ galaxy with a foreground source, but based on the present data we cannot exclude that the two blobs detected by HST are all at $z \geq 3$, and this could be an example of a stellar-powered LyC emission. A detail analysis of the VUDS spectrum indicates that the redshift of this source is only based on a noisy Lyman-α and strong CIV and SiIV lines, all in absorption. There are also other absorption lines, which are not associated with the $z = 3.32$ solution, but it was not possible to derive a secure redshift from these lines. Moreover, this source has strange colours ($u-g = 0.13$, $g-K = 2.87$ and $K-8.0\,\mu\mathrm{m} = 1.94$), which are not typical of a $z \sim 3$ star-forming galaxy. Indeed, the Ultravista data release 1 (DR1) catalogues by Ilbert et al. (2013) and Muzzin et al. (2013) give a photometric redshift of 0.596 and 0.628, respectively, for this object. Further analysis of this very peculiar source will be crucial to understand its nature.

4.1.2. Galaxies with $f_{\rm esc}^{\rm rel} < 100\%$ but detected LyC emission

In Table 1 there are six additional galaxies with detection in the LyC wavelengths and estimated values of $f_{\rm esc}^{\rm rel} \leq 100\%$.

A careful analysis of the LBC images in the *U*- and the *R*-bands, complemented by the HST imaging in the *I814W* band, allows us to distinguish between real LyC emission and foreground contamination. Four (ID = 19521, 40998, 48734, and 47357) out of these six sources show a situation similar to the four previously analysed galaxies: the high spatial resolution images by HST (Fig. A.2) show the presence of possible faint contaminants with spatial offsets from the spectroscopically identified galaxies at $z \sim 3.3$. To check if they are foreground galaxies, we adopt, as in the previous cases, the test of the local escape fraction to verify if it is consistent with the emission from plausible stellar populations and with the IGM attenuation. We computed the escape fraction restricting the area to the region covered by the LyC emission in the *U*-band, instead of computing the fluxes in the region defined by the non-ionizing band (in this case the LBC *R*-band). For all of these four galaxies, the escape fraction computed locally on the *U*-band emission further exceeds the physical limit of 100%, in some cases reaching 600% or more (see notes to Table 1).

For the remaining two galaxies (ID = 25155 and 63327) the presence of a contaminating foreground is not obvious from HST data, and their local escape fractions are <100% if we limit the analysis to the region with *U*-band emission. The galaxy 25155 (Fig. 3) is isolated and we only find a hint of a very faint blob slightly offset from the $z = 3.3$ galaxy if we carefully check the HST *I814W* image. This blob has a distance of 0.1 arcsec from the bright object, thus it is very hard to draw

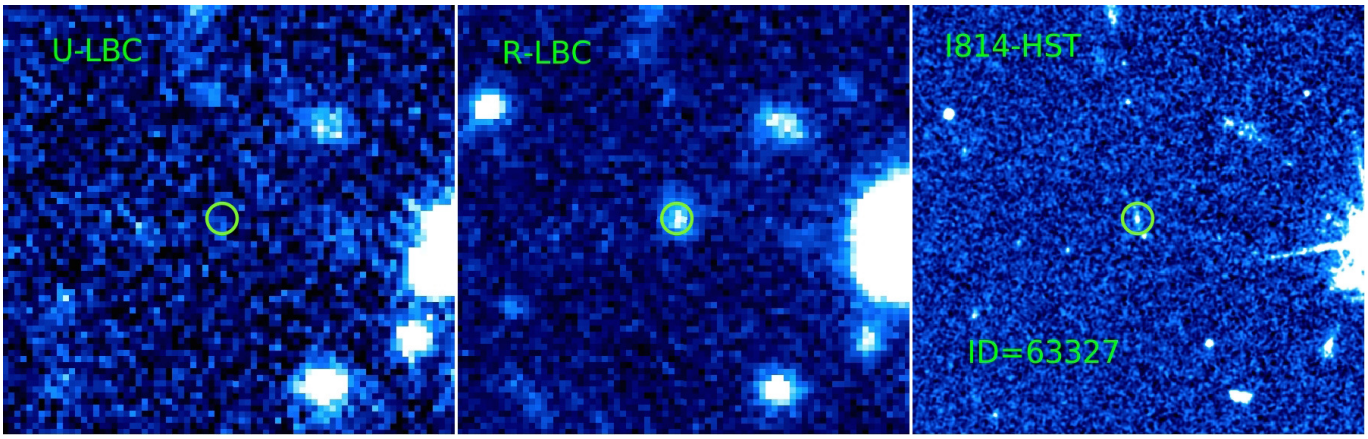

Fig. 4. Cutouts of source ID = 63327 in the U-band (*left*) and in the R-band (*centre*) by the LBC instrument. The cutout on the *right* shows the same sky area observed by HST in the *I814W* filter. The position of the spectroscopic redshift is indicated with a green circle. The size of the cutouts is 15 arcsec. In the HST image there is a faint blob towards the south-west, but it is blended with the galaxy at $z \sim 3.33$ in the LBC R-band. In the LBC U-band there is a very faint emission slightly offset towards the south w.r.t. the R-band position.

any conclusions on its true nature. We assume in the following that it could be a genuine LyC emitter at $z \sim 3.3$. This galaxy has a relatively faint magnitude $U = 28.6$ and it is marginally detected in the LBC COSMOS U-band image at $S/N = 2.2$, with a resulting escape fraction of ∼48%. Its optical spectrum by the VUDS survey shows typical absorption lines of high-z galaxies (Ly-α, SiIV, CIV) so it could resemble the "Ion1" source discussed in Vanzella et al. (2012a, 2015).

In addition, the detected U-band flux for galaxy ID = 63327 cannot be clearly explained by the presence of a lower redshift object contaminating the $z \sim 3.3$ source's LoS. We have thus another example of a plausible ionizing source by stellar radiation, with $f_{\rm esc}^{\rm rel} = 44.6\%$ and a marginal detection at $U = 28.5$ at $S/N = 2.2$. Figure 4 shows this source in the LBC U-band (left), in the LBC R-band (centre), and in the *I814W* band by HST (right). The HST image shows two blobs separated by ∼0.7 arcsec, but even at this high resolution we cannot judge whether this is a unique object or two distinct galaxies. There is still the possibility that there is a foreground contaminant roughly aligned with the $z \sim 3.3$ galaxy making an apparent blend that is indistinguishable even from HST data. To further exploring this possibility, we used the high resolution of the HST *I814W* image to carry out a de-blended photometry both in the U- and in the R-band with ConvPhot, as described in the previous sections, but now adopting the HST image as a prior. We obtain an upper limit of $U \geq 29.4$ at 1σ for the northern blob, while for the southern region we get a marginal detection $U = 28.9$ at 2σ. Translating the latter value into an escape fraction, we obtain $f_{\rm esc}^{\rm rel} = 119\%$, thus indicating that this can be a lower redshift interloper, similar to those discussed in the previous section. However, since this value of the escape fraction can be lower than 100% for slightly bluer stellar populations or a more transparent LoS, we still consider this object as a candidate LyC emitter, requiring further analysis in the future. We also checked the VUDS spectrum of this source looking for possible absorption features that are not consistent with the redshift of the $z \sim 3.3$ object, but the S/N is too low to carry out this test. Its optical spectrum only shows a relatively narrow Lyman-α in emission, with a symmetric profile. Deep UV images with HST or deep NIR spectroscopy could finally reveal its nature, as recently shown by Siana et al. (2015) for similar cases in the SSA22 area.

Summarizing, we have found evidence of contamination in 8 out of 45 cases (18%). This fraction is slightly larger than, but still consistent with the expected fraction of contamination (12–15%) derived following Vanzella et al. (2010a), assuming a depth of $U = 28.5$–29.5 and a seeing of 1.0 arcsec. We can thus conclude that there is a high probability that these eight galaxies detected in the U-band are all foreground interlopers.

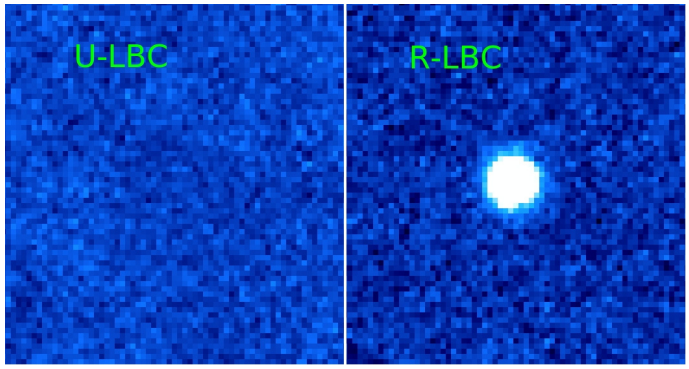

Fig. 5. Stack of the 37 galaxies with $3.27 < z_{\rm spec} < 3.40$ in the U (*left*) and R-bands (*right*) for the VUDS-LBC/COSMOS, Q0933, and Q1623 fields. Other objects detected in the R-band, but not associated with the galaxies at $z \sim 3.3$ (at the centre of the thumbnail) have been masked both in the U- and in the R-band image using the segmentation map derived from the R-band. The size of each image is 14 arcsec by 14 arcsec.

5. Results

5.1. The escape fraction derived on stacked images

We derived the stacked images in the U- and R-bands for the 37 galaxies presented in Table 1 indicated with the label Cont = No, excluding the eight galaxies where we have an evidence of possible foreground contamination, to measure the mean escape fraction of the population of star-forming galaxies. We included the two galaxies (ID = 25155 and ID = 63327) with marginal detection in the U-band in the stack. We adopted the same technique described in Boutsia et al. (2011). In summary, we extract a thumbnail of ∼45 arcsec × 45 arcsec centred around the $z \sim 3.3$ galaxies in the U- and R-band images by LBC, detect all the sources in the R-band, and mask all of them in both bands, except for the central target. Then, we average all the thumbnails of the 37 galaxies using the inverse square rms map as a weight. No clipping has been applied during the

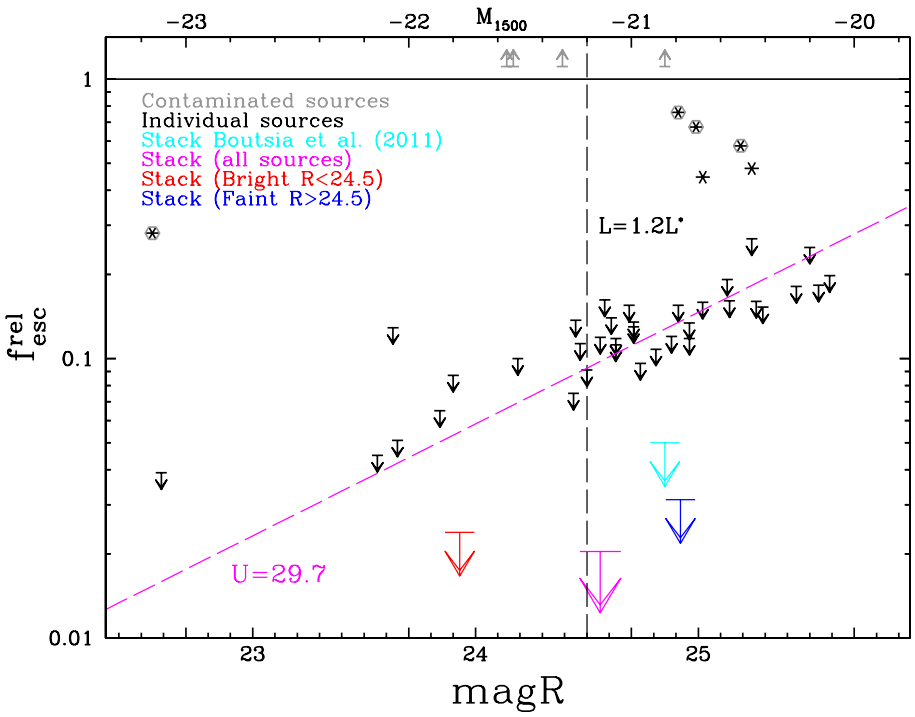

Fig. 6. Measured values and upper limits at 1σ for the LyC relative escape fraction of galaxies at $z \sim 3.3$ in the COSMOS field. Black descending arrows show the upper limits associated with individual galaxies, while the cyan arrow is the limit derived in Boutsia et al. (2011) by stacking 11 galaxies. The red arrow is the limit derived using only relatively bright galaxies with $R \leq 24.5$, corresponding roughly to $L \geq 1.2L^*$ ($M_{1500} \leq -21.2$). The blue arrow shows the upper limit for fainter galaxies (stack of 26 objects), while the magenta arrow indicates the upper limit for the whole sample (stack of 37 galaxies). The magenta dashed line is the expected $f_{\rm esc}^{\rm rel}$ for a limit in the U-band of 29.7 mag (at $S/N = 1$, assuming an intrinsic ratio $L_{1500}/L_{900} = 3$ and a mean IGM transmission of 0.28). This shows that the trend in larger escape fractions with fainter R-band magnitudes is due to the depth of the LBC image in the U-band, and it is probably not due to a physical trend in the population of star-forming galaxies. Asterisks show the galaxies with detection in the U-band and a significant LyC emission. The grey hexagons and the upper arrows indicate likely foreground contamination, where the global or the local escape fractions exceed 100%. Only two sources (ID = 25155 and ID = 63327, black asterisks without the grey hexagons) are examples of possible LyC emitters.

stacking. The resulting images (zoomed) are shown in Fig. 5. The high S/N in the stacked R-band image is immediately clear, given that each individual source is detected at $S/N > 10$ in the original frame. It is also evident that no detection is apparent in the U-band stack.

To be more quantitative, we adopted the same method described in the previous section for the individual sources, namely, we used the ConvPhot software to carry out a careful evaluation of the depth of the stacked images. The stacked source in the R-band has a mean magnitude of $R = 24.56$ with a $S/N = 283$. On the other hand, for the U-band we can only derive an upper limit to the emitted flux, reaching $U = 31.4$ at $S/N = 1$ (or equivalently $U = 30.2$ at $S/N = 3$). This translates into a lower limit for the flux ratio of $(F_R/F_U)_{\rm obs} = 545.1$, corresponding to an upper limit to the relative escape fraction of $f_{\rm esc}^{\rm rel} \leq 2.0\%$ at 1σ, or equivalently 6.0% at the 99.7% confidence level. If we exclude from the stack the two sources ID = 25155 and ID = 63327, i.e. the galaxies detected individually in the U-band at $\sim 2\sigma$ level, the previous results are not affected at an appreciable level. The stack of the 35 sources indeed gives a limit to the flux ratio of 549.5, corresponding to a similar limit for the escape fraction of 2.0% at 1σ. Thus the inclusion of two faint galaxies with marginal detection in the LyC does not modify the actual limit reached by the stacking.

We split the whole sample in different subsamples. We explore the escape fraction for the bright and faint subsamples. Considering the eleven galaxies with $R \leq 24.5$ within the total sample of 37 objects used above, we end up with a weighted-mean magnitude of $R = 23.93$ and an upper limit for the escape fraction of 2.4% at 1σ. The stack of the remaining 26 sources with $R > 24.5$ instead gives a weighted mean of $R = 24.92$ and $f_{\rm esc}^{\rm rel} \leq 3.1\%$ at 1σ (or equivalently $f_{\rm esc}^{\rm rel} \leq 9.4\%$ at 3σ level). In this case, the slightly worse limit to the LyC escape fraction is only because of the faintness of the subsample.

Table 2. Escape fraction of stacks.

Sample	$N_{\rm gal}$	R mag (AB)	$f_{\rm esc}^{\rm rel}$ (1σ)
Bright ($R \leq 24.5$)	11	23.93	≤0.024
Faint ($R > 24.5$)	26	24.92	≤0.031
All sources	37	24.56	≤0.020

Figure 6 shows the escape fraction at 1σ as a function of the observed R-band magnitudes for all individual sources and for the stacks. The trend of larger $f_{\rm esc}^{\rm rel}$ with fainter R-band magnitudes is simply due to the depth of the LBC image in the U-band ($U = 29.7$ AB mag at $S/N = 1$), and it is not due to a physical trend in the galaxy population (i.e. higher escape fraction for fainter sources).

The results of the stacks are summarized in Table 2 and are also plotted in Fig. 6 with magenta, red, and blue arrows for the total sample and the bright and faint subsamples, respectively. These limits are a factor of 2.5 more stringent than the previous results by Boutsia et al. (2011), and demonstrate the power of stacking a large sample of galaxies to reach very deep constraints to the ionizing escape fraction at $z \sim 3.3$.

5.2. UV Background from star-forming galaxies at $z \sim 3$

Using the results obtained in the previous section, we can now derive a constraint for the UV background (*UVB*) produced by the population of star-forming galaxies at $z \sim 3$. We derived the luminosity density at 900 Å rest frame as in Boutsia et al. (2011), starting from the analogous quantity at 1500 Å rest and correcting it for the intrinsic slope of the spectrum of these galaxies

Table 3. HI photoionization rate for different LF parametrization and integration limits.

f_{esc}^{rel}	LF	α	$\Gamma_{-12}(M_{1500} \leq -20.2)$ $L \geq 0.5\ L^*$	$\Gamma_{-12}(M_{1500} \leq -17.2)$ $L \geq 0.03\ L^*$	$\Gamma_{-12}(M_{1500} \leq -14.2)$ $L \geq 0.0016\ L^*$
<2%	Reddy & Steidel (2009)	–1.73	< 0.12	<0.38	<0.93
<2%	Sawiki & Thompson (2006)	–1.43	< 0.10	<0.23	<0.31
<2%	Cucciati et al. (2012)	–1.50	<0.10	<0.19	<0.26
<2%	Cassata et al. (2011)	–1.78	–	<0.08[a]	–
21%	Reddy & Steidel (2009)	–1.73	1.24	3.94	9.73

Notes. The upper limits on f_{esc}^{rel} and Γ_{-12} are at 1σ. [(a)] Cassata et al. (2011) found a star formation rate density of 0.008 $M_\odot$/yr/Mpc^3 integrating the LAE LF down to $0.04L^*$. This SFR density is a factor of 5 below that by Reddy & Steidel (2009).

(adopting $L_{1500}/L_{900} = 3$) and the derived limit for the escape fraction of 2%, i.e.

$$\rho_{900}^{esc} = \rho_{1500} \cdot f_{esc}^{rel} \cdot (L_{900}/L_{1500})_{int}. \quad (3)$$

As derived from Eq. (1), the product $f_{esc}^{rel}(L_{900}/L_{1500})_{int}$ is equivalent to $(F_U/F_R)_{obs}\exp(\tau_{IGM})$, which are measured quantities less subject to systematic uncertainties or assumptions.

The only parameter affecting these calculations is the input luminosity density of non-ionizing radiation, ρ_{1500}. To obtain this value it is sufficient to integrate an observed LF, multiplied by the absolute luminosity, down to a specific magnitude limit. We decided to adopt the parametrization of Reddy & Steidel (2009) for the LF at $z \sim 3$ after converting it from 1700 to 1500 Å rest-frame wavelengths, as described in Boutsia et al. (2011). We adopt a slope of $\alpha = -1.73$ and integrate down to an absolute magnitude of $M_{1500} = -20.2$, which is equivalent to $L \sim 0.5\ L^*(z = 3)$. We choose this limit since it corresponds to the limiting magnitude of our sample, $R \sim 25.5$. The resulting luminosity density is $\rho_{1500} = 1.27 \times 10^{26}$ erg s^{-1} Hz^{-1} Mpc^{-3}. Adopting an upper limit for the escape fraction of ≤2.0%, we obtain a limit to the ionizing emissivity of $\rho_{900}^{esc} \leq 0.85 \times 10^{24}$ erg s^{-1} Hz^{-1} Mpc^{-3} at 1σ level, or equivalently $\rho_{900}^{esc} \leq 2.55 \times 10^{24}$ erg s^{-1} Hz^{-1} Mpc^{-3} at 3σ.

We can translate this ionizing luminosity density into a metagalactic hydrogen photoionization rate Γ_{-12}, (ionization rate of HI in unit of 10^{-12} s^{-1} atom^{-1}) using the formula by Meiksin (2009) and Mostardi et al. (2013),

$$\Gamma_{-12} = \frac{10^{12} \cdot \rho_{900}^{esc} \cdot \sigma_{HI} \cdot \Delta l \cdot (1+z)^3}{h_P \cdot (3 + |\alpha_{UV}|)}, \quad (4)$$

where $\sigma_{HI} = 6.3 \times 10^{-18}$ cm^2 is the hydrogen photoionization cross section at $\lambda = 912$ Å, $\alpha_{UV} = -3.0$ is the spectral slope of the stellar ionizing radiation (from Mostardi et al. 2013), and h_P is the Planck constant. The mean free path of ionizing photons, Δl is 83.5 proper Mpc at $z = 3.3$, according to recent estimates by Worseck et al. (2014a). The 1σ uncertainty in Δl at $z = 3.3$ is 4.8 Mpc (i.e. 6%). The uncertainties in the emissivity of galaxies at 1500 Å rest frame (due to the uncertainties in the parametrization of the galaxy LFs) are thus dominating the source of errors in Γ_{-12}, as shown in Table 3. In the next section, we discuss the implications of different parametrization of the galaxy LFs on the HI photoionization rate.

Following Faucher-Giguère et al. (2009), at $z \sim 3$ the galaxy radiation can be considered rather uniform, and in this case the net effect of discrete absorbers is a hardening of the emissivity, caused by the IGM filtering. As a consequence, a correct value for galaxies can be $\alpha_{UV} = -1.8$ (from Appendix D of Faucher-Giguère et al. 2009), which is in agreement with the value provided by Haardt & Madau (2012, see their Fig. 10).

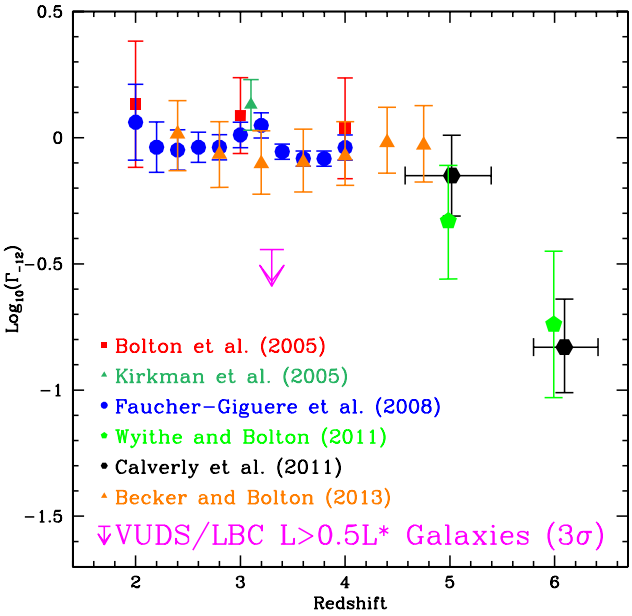

Fig. 7. Evolution of the *UVB*, $\log_{10}(\Gamma_{-12})$, as a function of redshift. These measurements are typically derived by an analysis of the Lyman forest properties or by the proximity effect. The 3σ upper limit from this work ($\Gamma_{-12} \leq 0.36$) is indicated with a magenta arrow. This limit, obtained by star-forming galaxies with $L \geq 0.5L^*$ at $z \sim 3.3$, shows that the bright galaxies alone cannot be responsible for the *UVB* at this redshift.

We thus obtain an upper limit $\Gamma_{-12} \leq 0.12$ at 1σ (or 0.36 at 3σ) for the ionization rate of relatively bright ($M_{1500} \leq -20.2$, or $L \geq 0.5L^*$) star-forming galaxies at the mean redshift of our sample ($z = 3.3$). For comparison, a recent estimate of the ionization rate by Becker & Bolton (2013) gives $\Gamma_{-12} = 0.79^{+0.28}_{-0.19}$ at $z = 3.2$, well above our limit. Figure 7 shows the derived upper limit (at 99.7% c.l. or 3σ) for Γ_{-12} from the VUDS-LBC/COSMOS data, compared with recent determinations of the *UVB* in the literature. These estimates are derived through an analysis of the Lyman-α forest properties (Bolton et al. 2005; Kirkman et al. 2005; Faucher-Giguère et al. 2008; Wyithe & Bolton 2011; Becker & Bolton 2013) or by the proximity effect (Calverley et al. 2011). We scaled the data shown in Fig. 7, derived from flux decrement analysis in the IGM Lyman forest of QSO spectra (Bolton et al. 2005; Faucher-Giguère et al. 2008; Wyithe & Bolton 2011), to the same cosmology and to the same IGM temperature-density relation, as described in Calverley et al. (2011) and in Giallongo et al. (2012). It is clear from this plot that the ionizing emission of relatively bright ($L \geq 0.5L^*$) star-forming galaxies is insufficient to keep the Universe reionized at $z \sim 3.3$ at more than 99.7% probability. The recent determinations of Becker & Bolton (2013) take a series of systematic

effects on the derivation of Γ_{-12} into account, and thus their error bars can be considered as a robust estimates for the uncertainties in the UVB. Our upper limit is clearly lower than their minimum envelope, which is a convincing argument against a major contribution of bright star-forming galaxies to the ionizing emissivity at $z = 3$. In the next section, we discuss in detail the possible way out for the missing HI ionizing photons at $z \sim 3$.

6. Discussion

Our results are based on two main assumptions, namely the mean IGM transmission $\langle \exp(-\tau_{\rm IGM}) \rangle$ and, in a more subtle way, the adopted value for the intrinsic ratio $(L_{1500}/L_{900})_{\rm int}$. We discuss in the following sections the implications of the choice of these two parameters on our conclusions.

6.1. The variance of the IGM and ISM transmissions

In the previous sections, we adopted a mean value of 0.28 for the mean IGM transmission close to the Lyman limit. This value however is subject to large cosmic variance due to differences in the absorption patterns in various LoS, especially as a result of the patchy nature of the LLs and DLAs, which are able to block the path of ionizing photons through the IGM. The IGM absorption at ~900 Å is thus very stochastic because it is related to the probability of intercepting dense absorbers, with $\log(N_{\rm HI}) \geq 17$.

We estimated the variance of the IGM transmission $\exp(-\tau_{\rm IGM})$ at ~900 Å rest frame, adopting the Monte Carlo simulations of Inoue & Iwata (2008) and the recent updated absorber statistics by Inoue et al. (2014) used also by Vanzella et al. (2015). Recently, Thomas et al. (2015) estimated the same quantity using deep VUDS spectra of galaxies in the redshift interval $2.5 \leq z \leq 5.5$, finding an excellent agreement with the IGM transmission obtained from quasars' LoS at $z \leq 4$. We considered 10 000 different realizations of the IGM transmission at $z \sim 3.3$ and convolved each of them with the profile of the LBC U-band filter, thus obtaining a mean transmission and its variance. We obtained a mean value of $\langle \exp(-\tau_{\rm IGM}) \rangle = 0.25$, similar to the adopted value of 0.28 based on the Worseck et al. (2014a) IGM transmission, and a dispersion of ~0.2. The resulting distribution of IGM transmission at $z \sim 3.3$ is asymmetric, with a tail towards low $\exp(-\tau_{\rm IGM})$ because of the presence of DLAs and LL systems. A fraction of 11% of all the simulated LoS shows a transmission $\exp(-\tau_{\rm IGM})$ less than 0.01, thus it is important to have a large number of galaxies with measured LyC escape fraction to minimize the stochastic effect of intervening absorbers. Considering our case of 37 different LoS, the dispersion of $\langle \exp(-\tau_{\rm IGM}) \rangle$ is 0.03.

Another source for the skewed probability distribution function towards low values of the escape fraction of galaxies is the patchiness of the ISM, which has been recently explored by Cen & Kimm (2015). Using high-resolution, large-scale simulations with radiative transfer calculations, these authors show that LyC photons can escape from a galaxy through small solid angles with complete transparency, while the majority of the remaining LoS are opaque. Adopting their simulations at $z = 4$ and at a virial mass $10^{10} \leq M \leq 10^{11} M_{\odot}$, we estimate that for an input escape fraction of 2% for 37 galaxies, the confidence interval at 1σ level is between $f_{\rm esc}^{\rm rel} = 1.4\%$ and 2.7%. Simulations are not available for our redshift and virial mass range, but the trend in redshift and masses derived by Cen & Kimm (2015) shows that our extrapolation at $z \sim 3.3$ and higher luminosities should be fair enough. Combining the uncertainties as a result of both the stochasticity of the IGM and the variance of the ISM in different LoS, the confidence interval at 1σ is between $f_{\rm esc}^{\rm rel} = 1.3\%$ and 2.8%.

Thus we can conclude that with our relatively large sample of galaxies we are able to limit the variance due to both IGM transmission and patchy ISM of the star-forming galaxies. We can exclude that the lack of ionizing photons we observed in the VUDS-LBC/COSMOS sample is due to low number statistics and variance in the IGM or ISM transmission. In the near future, the combination of HST imaging, deep UV observations, and large spectroscopic surveys will provide more than 100 galaxies in which these measurements can be repeated.

6.2. The intrinsic ratio $(L_{1500}/L_{900})_{\rm int}$

Our choice of the $(L_{1500}/L_{900})_{\rm int}$ ratio does not enter directly into the evaluation of the total ionizing emissivity since the dependencies of $\rho_{900}^{\rm esc}$ from the intrinsic ratio $(L_{1500}/L_{900})_{\rm int}$ is cancelled out, once Eqs. (1) and (3) are combined. As we have already discussed, in fact, the value of the HI photoionization rate only depends on the observed ratio between the U- and the R-band photometry and on the IGM correction. However, the $(L_{1500}/L_{900})_{\rm int}$ ratio can be used to provide us with a physical interpretation of the amount of UV ionizing photons escaping from a galaxy, and enters into our definition of the sample. We discuss this latter aspect here.

The relative escape fraction derived for our sample of star-forming galaxies assumes a given ratio between the intrinsic luminosity at 1500 and 900 Å rest frame, here taken to be $(L_{1500}/L_{900})_{\rm int} = 3$. This value has been adopted for a direct comparison with previous works dealing with similar subjects (Steidel et al. 2001; Shapley et al. 2006). The intrinsic ratio $(L_{1500}/L_{900})_{\rm int}$ depends on the SFH, stellar populations, age, metallicity, IMF of the investigated galaxies.

Vanzella et al. (2010b) showed that the intrinsic value $(L_{1500}/L_{900})_{\rm int}$ can be ≤ 7 if considering mean values for the physical parameters of high-z, star-forming galaxies. Adopting this new value would approximately double the escape fraction we measured for the VUDS-LBC/COSMOS sample, but would not change our conclusions concerning their contribution to the ionizing emissivity. Moreover, adopting a value of 7 for $(L_{1500}/L_{900})_{\rm int}$ would result in even higher values for the relative escape fraction of the galaxies, which already show $f_{\rm esc}^{\rm rel} \geq 100\%$, thus strengthening our conclusions about their nature of low-redshift interlopers.

Alternatively, Topping & Shull (2015) adopted a recent rendition of stellar evolutionary tracks as input in their galaxy synthesis model, finding a 50% increase in the LyC production efficiencies w.r.t. previous calculations. Changing the intrinsic value of $(L_{1500}/L_{900})_{\rm int}$ to 2 would not change our conclusions concerning the ionizing emissivity, as discussed above. Moreover, since the relative escape fraction we derived with the local method is significantly greater than 100% (175–966%) for all the galaxies considered to be affected by foreground contamination, a correction of 50% downward would only partially alleviate the tension for one object (ID = 19521), but would not solve the problem for the other galaxies.

We can thus conclude that the assumed value of $(L_{1500}/L_{900})_{\rm int} = 3$ does not significantly affect our conclusions concerning the ionizing emissivity of star-forming galaxies at $z \sim 3.3$.

6.3. Comparison with other results

According to Cooke et al. (2014), the LBG selection could be biased against LyC sources, since a galaxy with significant emission at $\lambda \leq 912$ Å rest frame would avoid the classical dropout selection. We show here that our sample is not affected by these systematics. In fact, even assuming an escape fraction of 100% and a completely transparent IGM (very unlikely), the typical colour of a galaxy at $z \sim 3$ would be $U - R \geq 1.2$, above the colour criteria normally adopted to select candidate galaxies for spectroscopic follow up (see for example Le Fèvre et al. 2015 and Boutsia et al. 2014). A recent paper (Vanzella et al. 2015) confirms our conclusions with state-of-the-art simulations adopting the updated recipes of Inoue et al. (2014) for the IGM transmission.

The result found from the VUDS-LBC/COSMOS sample can be compared with recent achievements on the detection of LyC emitters at $z \geq 3$. Iwata et al. (2009), Nestor et al. (2011, 2013), Mostardi et al. (2013) found a significant number of ionizing sources in their surveys. In the SSA22 area, Iwata et al. (2009) found evidence for $f_{\rm esc}^{\rm rel} > 4\%$ for the whole population of 73 LBGs analysed, but also provided evidence for a significant spatial offset between the ionizing and non-ionizing emission for some of them. Moreover, there are few objects detected in LyC with a flux ratio F_{1500}/F_{900} which is smaller than the typical values expected from young or old stellar populations (PopI/II) with standard Salpeter IMF (or others that are not top-heavy), even assuming a transparent IGM. Moreover, they did not carry out a local estimate of the escape fraction in the position of the detected LyC sources.

On the same SSA22 field, Nestor et al. (2011) and Nestor et al. (2013) show nine LBGs and 20 Lyman-α emitters (LAEs) with LyC detection out of a sample of 41 LBGs and 91 LAEs (all spectroscopically confirmed). They started from a different narrowband image centred at ~3640 Å, which is deeper than that used by Iwata et al. (2009), at ~3590 Å. A careful analysis of their LBG detections, however, shows that even in this case the LyC emission for many $z \sim 3$ sources is offset by 0.4–1.0 arcsec. The observed ratio between the 900 and 1500 Å rest-frame emission is difficult to reconcile with that expected by standard stellar populations (Vanzella et al. 2012a). The HST images in *I814W* filter available for a few of them show the presence of clearly separated galaxies, sometimes fainter at 1500 Å than in the ionizing continuum (i.e. their C16 object), with a resulting escape fraction well exceeding 1000% if estimated in the LyC position. For the majority of them, no HST imaging is available but even ground-based images often show the presence of slightly offset emission in LyC, w.r.t. the non-ionizing continuum. Similar conclusions can be reached for the Mostardi et al. (2013) sample where they adopt the same analysis as in Nestor et al. (2013). At $z \sim 2.8$, they found four LyC emitters out of 49 LBG galaxies and seven LyC emitters out of 91 LAEs. In this case the lack of high spatial resolution data from HST for the majority of the sample prevents any detailed analysis about possible contamination by interlopers/foregrounds. These conclusions have been strengthened by recent observations by Siana et al. (2015), who found no convincing detection in their deep HST imaging with WFC3-UVIS of five LyC emitters extracted from the sample of Nestor et al. (2011), or by Mostardi et al. (2015), who only found one robust LyC emitter after a reanalysis of a sample of 16 galaxies by Mostardi et al. (2013). More interestingly, the only robust candidate LyC emitter by Mostardi et al. (2015), the galaxy MD5b, has an observed ratio $F_{\rm UV}/F_{\rm LyC} = 4.0 \pm 2.0$, equivalent to a relative escape fraction of 75%, when assuming complete transmission of the IGM. Instead, if a mean value of $\langle \exp(-\tau_{\rm IGM}) \rangle = 0.4$ at $z \sim 3.1$ is adopted, following Inoue et al. (2014), the relative escape fraction of MD5b turns out to be 188%. Imposing the constraint of a physical value for the relative escape fraction of $f_{\rm esc}^{\rm rel} < 100\%$, the LoS of MD5b must be very transparent, $\exp(-\tau_{\rm IGM}) > 0.75$, which corresponds to a probability $<10^{-4}$, according to Inoue et al. (2014). This could be an indication that this galaxy is also a low-z contaminant, similar to the other cases studied by Mostardi et al. (2015).

If we compare the apparent statistic of LyC detections in VUDS, we have ten individual detections out of 45 galaxies (22%), similar to the value by Nestor et al. (2011), but significantly more than the value by Mostardi et al. (2013, 8%), probably because of their shallow narrowband imaging.

In summary, it is difficult to compare different results obtained through imaging of different quality in a homogeneous way in terms of depth and angular resolution. It appears however that the apparent discrepancies from different databases tend to converge towards low values for the average escape fraction if we remove the probable low-z contaminants from the analysis, i.e. the objects with flux ratios F_{900}/F_{1500} significantly higher than that predicted by spectral synthesis models, where a spatial offset between F_{900} and F_{1500} is present (Vanzella et al. 2012a; Siana et al. 2015).

6.4. The sources of ionizing photons at $z \geq 3$

In the previous section, we have shown that bright ($L \geq 0.5\,L^*$) galaxies at $z \sim 3.3$ cannot alone provide the required LyC emissivity ($\Gamma_{-12} < 0.36$ at 99.7% confidence level) to explain the measured *UVB*. The AGN contribution at $z = 3.3$ is $\Gamma_{-12} = 0.37$ (from Fig. 8a of Haardt & Madau 2012). The measured value at $z = 3.2$ is $\Gamma_{-12} = 0.79^{+0.27}_{-0.19}$ according to Becker & Bolton (2013). Even considering the uncertainties, there is a tension between the measured value of Γ_{-12} and the summed contributions of AGNs plus bright galaxies at $z = 3.3$. This implies that an additional source of ionizing photons ($\Gamma_{-12} = 0.06 - 0.33$) is probably required to reach the observed value of the photoionizing background, taking its uncertainties into account. Looking for ionizing sources among the fainter galaxy population is the obvious next step. The faint population is more numerous and could show a higher average escape fraction (Razoumov & Sommer-Larsen 2010; Alvarez et al. 2012; Fontanot et al. 2014; Paardekooper et al. 2013, 2015; Kimm & Cen 2014; Wise et al. 2014; Roy et al. 2015; Duncan & Conselice 2015). In the following, we explored different combinations of the escape fraction, slope α of the LF, and magnitude limit M_{1500}, which are adopted to compute the ionizing emissivity, looking for the sources responsible for the observed *UVB* at $z \sim 3.3$. A summary is provided in Table 3.

Adopting very steep LFs as derived by Reddy & Steidel (2009) with a power-law index $\alpha = -1.73$, and integrating down to $M_{1500} = -17.2$ (or $R = 28.5$), we obtain an ionization rate of $\Gamma_{-12} \leq 0.38$ at 1 σ, assuming a constant escape fraction of 2%, as for the brighter galaxies.

The relative escape fraction of galaxies brighter than $M_{1500} \sim -20.2$ ($L = 0.5L^*$) should be ~16% to provide a photoionization rate $\Gamma_{-12} \sim 0.95$, in agreement with the observed value at $z \sim 3$, shown in Fig. 7. Alternatively, the escape fraction can remain at approximately a few percent, but the LF must be integrated down to very faint magnitudes, at $M_{1500} = -14.2$ (Fontanot et al. 2014; Alavi et al. 2014) to yield $\Gamma_{-12} \sim 0.9$. The calculations above are quite conservative, since we are assuming a rather steep LF ($\alpha = -1.73$). At $z \sim 3$ the estimated slopes of the

galaxy LF are generally flatter, with $\alpha \sim [-1.4, -1.5]$ (Sawiki & Thompson 2006; Finkelstein et al. 2015; Parsa et al. 2015), with the exception of the LF of LAEs by Cassata et al. (2011), which has $\alpha \sim -1.8$ at $z \geq 3$. Adopting the parametrization of Sawiki & Thompson (2006), with $\alpha = -1.43$, and integrating down to $M_{1500} = -14.2$, the ionizing emissivity is $\Gamma_{-12} \leq 0.31$, which is insufficient to keep the Universe reionized. Similarly, if we adopt the LF by Cucciati et al. (2012) with a slightly steeper slope ($\alpha = -1.50$), but brighter M^*, we find an emissivity of $\Gamma_{-12} \leq 0.26$ at $M_{1500} = -14.2$, far from providing enough ionizing photons to maintain the reionization of the Universe. The latter LF is based on the VVDS (Le Fèvre et al. 2013) spectroscopic survey, so it should be robust against interlopers in the $z \sim 3$ LF. At $z \geq 3$, Cassata et al. (2011) find that the LF of LAEs is relatively steep, with a slope of ~ -1.8. However, these galaxies are much fainter than the typical UV selected galaxies discovered at the same redshifts. They measured a star formation rate density, which is a factor of 5 lower than that by Reddy & Steidel (2009), with the implication of a lesser contribution of the LAEs to the HI ionizing background at $z \sim 3$. Table 3 summarizes the different HI photoionization rates derived for different parametrization of the $z \sim 3$ galaxy LF and at different luminosities.

In comparison with other works (e.g. Iwata et al. 2009; Nestor et al. 2011; Mostardi et al. 2013), we have carried out the stacking of all the 45 sources in Table 1, regardless of the contamination by possible foreground sources. In this case, we have a clear detection in the U-band with $S/N = 11$, of $U = 28.87$. This translates into an escape fraction of $f_{\rm esc}^{\rm rel} = 21\%$, in agreement with previous findings of Iwata et al. (2009), Nestor et al. (2011), Mostardi et al. (2013). The resulting ionizing emissivity of $L \geq 0.5L^*$ galaxies (or equivalently $R \leq 25.5$, our limit) is $\Gamma_{-12} = 1.24$, and, thus, all the LyC photons measured in the Lyman forest should be provided by relatively bright galaxies, with the consequence of a negligible contribution by fainter galaxies or by AGNs. Taken at face value, this would imply that only galaxies brighter than $\sim 0.5\ L^*$ are contributing to the ionizing radiation at $z \sim 3.3$, thus excluding fainter galaxies and the QSO/AGN population as sources of ionizing photons. This is at variance with the conclusions of Lusso et al. (2015) and Glikman et al. (2011), who found that bright QSOs at $z \sim 2.4$ and at $z \geq 4$, respectively, should provide at least $\sim 50\%$ of the HI ionizing photons.

If we integrate the Reddy & Steidel (2009) LF down to $M_{1500} = -17.2$, corresponding to a limit of $R = 28.5$, and then compute the escaping emissivity at 900 Å rest frame assuming $f_{\rm esc}^{\rm rel} = 21\%$, we end up with $\Gamma_{-12} = 3.94$, which is well above the measured value at $z = 3.3$ shown in Fig. 7. We can thus conclude that a large fraction of the galaxies with detected LyC emission in the VUDS-LBC/COSMOS field are plausibly contaminated by foreground interlopers, as discussed above and also shown by Siana et al. (2015) and Mostardi et al. (2015). In this case, star-forming galaxies alone are probably not able to keep the Universe ionized at $z \sim 3.3$. The situation can be different at higher redshifts.

Recent evaluations by Finkelstein et al. (2015) and Bouwens et al. (2015a) show a steepening of the faint end of the LF with a slope as steep as -2 at $z \sim 6$–7, i.e. close to the epoch of reionization. Very high-redshift, star-forming galaxies down to $M_{1500} = -17$ at $z \sim 7$ could ionize the IGM if they had an escape fraction of $\sim 13\%$. Similarly, Bouwens et al. (2015b) modelled the redshift evolution of the ionizing emissivity integrating the LF of star-forming galaxies down to $M_{1500} \sim -13$ and assuming an escape fraction of 0.10–0.40. These parametrizations allowed them to reproduce the observed trend in the ionization rate $\dot{N}_{\rm ion}$ inferred at $z > 6$ by a number of independent observations (see their Table 1). Using the same approach, Duncan & Conselice (2015) concluded that star-forming galaxies at $z > 6$ down to $M_{1500} \sim -15$ and with $f_{\rm esc} \sim 0.16$–0.42 could complete and maintain the reionization process. Given our limits, ($f_{\rm esc}^{\rm rel} \leq 2\%$) at $z \sim 3.3$, an increase in the escape fraction should be invoked for star-forming galaxies with lower luminosities and/or increasing redshifts to make these sources the major contributors to the reionization at $z > 6$. The observational evidence that galaxies at higher redshifts and fainter luminosities are bluer and less dusty than bright and low-z galaxies (Duncan & Conselice 2015) and the recent finding that ionization parameter can be higher for $z > 6$ galaxies (Stark et al. 2015), may indicate that high-z galaxies can be more efficient ionizing agents than galaxies at $z < 3$.

The alternative possibility that the AGN population can provide most of the ionizing flux in the Universe cannot be excluded, however. Faint multi-wavelength surveys based on very deep near infrared data and at the same time ultra-deep X-ray images are discovering a population of faint AGNs at very high redshifts ($z \sim 4$–7), which could provide the required ionizing photons (e.g. Fiore et al. 2012; Giallongo et al. 2012, 2015). The main uncertainty even for this population relies on the escape fraction of ionizing photons from their host galaxies. It is not clear whether the AGN escape fraction remains high for progressively fainter sources, but, at variance with the galaxy population, the brighter AGNs and QSOs having $f_{\rm esc}^{\rm rel} \sim 100\%$ are known to ionize their neighbourhood even at $z \sim 6$ (Worseck et al. 2014a). In the local Universe, recent results by Stevans et al. (2014) seem to indicate that even the faint AGN population has an escape fraction close to unity. Accurate measurements of the escape fraction of faint AGNs at $z > 3$ are important to confirm this hypothesis.

6.5. Comparison with theoretical predictions

Theoretical predictions of the ionizing photon leakage from star-forming galaxies at high-z are far from settled despite the large effort put into complex numerical simulations, and different conclusions were obtained by various authors on this subject in the past.

Using high-resolution simulations, Gnedin et al. (2008) derived an absolute escape fraction of ~ 1–3% for galaxies with mass $M \geq 10^{11}\ M_\odot$ and star formation rate ~ 1–$5\ M_\odot$/yr at $3 < z < 9$. This model is in slight agreement with our result on the VUDS-LBC/COSMOS region. They also predict that the escape fraction declines steeply at lower masses and SFR, while they found large variance among different LoS within individual galaxies. According to their model, a high-z galaxy can be more transparent along the galactic poles than through the galactic disk. They explain the low values of escape fractions with a small fraction of young stars located just outside the edge of the HI disk. In lower mass galaxies, this disk is thicker and more extended relative to the distribution of young stars compared to massive galaxies, causing a progressively lower escape fraction.

In contrast to Gnedin et al. (2008), the simulations of Yajima et al. (2014) found that $f_{\rm esc}^{\rm abs}$ remains roughly constant at a value of 20% (corresponding to $f_{\rm esc}^{\rm rel} = 52\%$ for $E(B-V) = 0.1$ and a Calzetti extinction law) from $z = 0$ to $z = 10$, and it does not show any clear dependence on the galaxy properties (i.e. luminosity). This is at variance with our results discussed in previous sections ($f_{\rm esc}^{\rm rel} \leq 2\%$ at $L \geq 0.5\ L^*$).

Using ray tracing simulations with spatial resolution of 3.8 pc, Ji-hoon et al. (2013) find $f_{\rm esc}^{\rm abs} = 1.1\%$ for a spiral

galaxy in a dark matter halo of $\sim 2\times10^{11}\ M_{\odot}$. They do not predict the dependence of the escape fraction from galaxy mass or luminosity. Models based on hydrodynamical simulations or radiative transfer calculations (Razoumov & Sommer-Larsen 2010; Paardekooper et al. 2013; Kimm & Cen 2014; Wise et al. 2014) generally predict an increase of the escape fraction at fainter luminosities or at lower halo masses, with a large value of the absolute escape fraction (∼15–80%) at $M_{1500} \sim [-14, -10]$ and at high redshifts ($z > 4$).

Only recently, however, the predictions from cosmological hydrodynamic simulations start converging on a general consensus that the escape fraction is increasing towards low masses/luminosities. For example, Paardekooper et al. (2015), using high-resolution cosmological hydrodynamic simulations of galaxy formation, find that only in 30% of the halos with $M_{200} = 10^8\ M_{\odot}$ (corresponding to a stellar mass of $\sim 10^5\ M_{\odot}$; see their Fig. 5, central panels) the absolute escape fraction is higher than 1% at $z > 9$, while $f_{\rm esc}^{\rm abs} \geq 10\%$ at $z = 6$ and/or at lower masses, with a strong anti-correlation between escape fraction and halo masses. Again, the population of ultra-faint galaxies in their model is essential in providing the LyC photons needed to sustain reionization. Our VUDS-LBC/COSMOS survey is limited to much brighter objects ($L \geq 0.5\ L^*$), thus we cannot provide meaningful constraints to those models. Using 2D hydrodynamic simulations, Roy et al. (2015) find $f_{\rm esc}^{\rm abs} \sim 5\%$ for Milky Way (MW) galaxies, with a trend in increasing the escape fraction for lower mass galaxies ($f_{\rm esc}^{\rm abs} \sim 10\%$ for galaxies ten times less massive than the MW).

Using high-resolution numerical simulations (0.1–4 pc) at $z \geq 6$, Ma et al. (2015) find a large time variability of $f_{\rm esc}^{\rm abs}$ (0.01–20%), with a mean value ≤5% over long timescales, without any strong dependence on mass or redshift. They also show that models based on sub-grid simulations, which are not able to resolve the star formation processes in dense molecular clouds, usually over-predict the HI ionizing escape fraction.

Phenomenological models (Haardt & Madau 2012; Kuhlen & Faucher-Giguère 2012; Alvarez et al. 2012; Fontanot et al. 2014) explored different parametrization of the escape fraction of high-z galaxies to explain the evolution of the UV background and the Thomson optical depth measured at that time by WMAP. They all assume a low escape fraction at $z \sim 3$, on the order of $f_{\rm esc}^{\rm abs} \sim 3$–$5\%$, but they require a strong evolution with luminosity or with redshift to fit the higher redshift data. The escape fraction of VUDS galaxies at $z \sim 3.3$ is still compatible (≤6% at 3σ level) with these values. More stringent limits and the exploration of the escape fraction at lower luminosities and/or higher redshifts can thus provide significant constraints to these models.

7. Summary and conclusions

We analysed the escape fraction of 45 galaxies selected in the COSMOS region (Scoville et al. 2007) with robust spectroscopic redshifts between $3.27 \leq z \leq 3.40$ from the ultra-deep VIMOS spectroscopic catalogue provided by the VUDS survey (Le Fèvre et al. 2015). Deep U- and R-band images obtained by LBC at the prime focus of the LBT telescope (observations described in Boutsia et al. 2014), reaching 1σ magnitude limits of $U \simeq 29.7$ and $R \simeq 28.2$, were used to measure the ionizing escape fraction from the galaxy sample down to a few percent level. The main results are the following:

- A subsample of ten galaxies with $R \leq 25.5$ has a measured U-band detection that corresponds to a LyC emission of $f_{\rm esc}^{\rm rel} \geq 28\%$. A detailed analysis of their properties has been performed computing the local escape fraction in the spatial region of the U-band where the supposed LyC flux was measured. Unphysical escape fractions $f_{\rm esc}^{\rm rel} \sim 300$–$1000\%$ have been derived for eight out of ten objects. The relative $f_{\rm esc}$ of these galaxies remains above 100% even assuming a transparent IGM and non-standard stellar populations/IMFs (PopIII or top heavy IMF).
- High-resolution HST images in the *I814W* band suggest that the supposed LyC emission comes usually from distinct interlopers slightly offset from the positions of the star-forming galaxies at $z \sim 3.3$. It turns out that eight out of the ten $z \simeq 3.3$ galaxies show detection in the LBC U-band contaminated by light from foreground galaxies at $z < 3$. Only two galaxies could be true LyC emitters, though the significance of their detection in the U-band is marginal, at 2σ level only, and for one of these two the possibility of contamination from an interloper is still open. Further observations of these peculiar sources will be fundamental to define their physical nature.
- We stacked the U- and R-band images of the remaining clean subsample of 37 galaxies at $z \sim 3.3$ (including the two marginal LyC detections) to compute their average ionizing escape fraction. The stacks are undetected in the U-band down to ∼31.4 mag (at 1σ). This corresponds to an upper limit of $f_{\rm esc}^{\rm rel} \leq 2\%$ (1σ) at $R \leq 25.5$ or equivalently $L \geq 0.5\ L^*(z = 3)$.
- Considering the stochasticity of the IGM and the patchiness of the ISM along different LoS as two sources of uncertainties for the derivation of the escape fraction, the relatively large number of galaxies analysed here, i.e. 37, allows us to constrain $f_{\rm esc}^{\rm rel}$ between 1.3% and 2.8% at 1σ confidence level.
- Integrating the Reddy & Steidel (2009) 1500 Å LF at $z \sim 3$ down to $0.5\ L^*$, we derived a significant upper limit to the ionizing emissivity and photoionization rate of relatively bright star-forming galaxies $\Gamma_{-12} \leq 0.12$ at 68% confidence level (corresponding to $\Gamma_{-12} \leq 0.36$ at 99.7% confidence level). This limit is a factor of two lower than the recent estimates derived from the IGM observed in the Lyman-α forest spectrum of bright QSOs at $z = 3$, as shown in Fig. 7. We can thus conclude that galaxies brighter than $0.5\ L^*$ give a small contribution to the *UVB* needed to keep the Universe ionized at $z \sim 3$.
- Our results differ from those obtained at similar redshifts by Iwata et al. (2009), Nestor et al. (2013), Mostardi et al. (2013). This is mostly because of the interpretation and quality of the database used. Robust spectroscopic redshifts are available for all the galaxies of our sample and high-resolution HST images supported by spectral synthesis models have been used to clean our sample from bona-fide low-redshift interlopers. Only few objects are currently genuine LyC emitters, and further analysis is important to understand their nature. Similar conclusions have been obtained by Vanzella et al. (2012a, 2015) in the GOODS-South field, by Siana et al. (2015) in the SSA22 area, and by Mostardi et al. (2015) in the HS1549+1933 field. Future NIR spectroscopic follow-up of all the faint interlopers can assess their nature.

In summary, considering that the expected AGN contribution at $z \sim 3$ amounts to $\Gamma_{-12} = 0.37$ (Haardt & Madau 2012), an additional contribution of $\Gamma_{-12} \sim 0.06 - 0.33$ is required to match the value of $\Gamma_{-12} = 0.79^{+0.28}_{-0.19}$ observed by Becker & Bolton (2013). This additional contribution could be provided

by a faint ($L < 0.5\,L^*$) galaxy population with an escape fraction of $f_{\rm esc}^{\rm rel} \geq 6{-}20\%$ (the exact value depends on the assumed slope of the galaxy LF), which is at least three times larger than our upper limit derived from the brighter population.

At higher redshifts ($z = 4{-}7$), where the contribution of bright AGNs to the photoionization rate is expected to be progressively less important (Haardt & Madau 2012), the escape fraction of star-forming galaxies is expected to be larger than the one measured here at $z \sim 3$. The galaxy LF at $z > 6$ is quite steep ($\alpha \leq -1.7$) compared to the LFs at $z \sim 3$ (e.g. Cucciati et al. 2012; Finkelstein et al. 2015; Bouwens et al. 2015a), and the contribution of faint galaxies (down to $M_{\rm UV} \sim -14$ with $f_{\rm esc}^{\rm rel} \sim 10{-}20\%$) is required to provide enough LyC photons to effectively contribute to the reionization of the Universe. This hypothesis however would imply a rapid change of the escape fraction of ionizing radiation from star-forming galaxies significantly fainter than L^*, which is difficult to explain in the current theoretical scenarios for galaxy formation and evolution (Ma et al. 2015). From the observational point of view, instead, there are indications that galaxies are bluer at high redshift and faint luminosities, thus plausibly implying younger and less absorbed stellar populations, with possible larger contribution of ionizing photons than those present at $z \sim 3$ (Stark et al. 2015; Bouwens et al. 2015b; Duncan & Conselice 2015). A significant contribution to the reionization by different populations is still possible, however, since the escape fraction of galaxies at $z = 4{-}7$ is currently a free parameter. Faint AGNs are the most plausible competitors (Giallongo et al. 2012, 2015; Worseck et al. 2014b), but more exotic alternatives, such as primordial cosmic rays, PopIII stars which are forming high-mass X-ray binaries, or Hawking evaporation of primordial mini black holes, could also play a role (Tueros et al. 2014; Belotsky & Kirillov 2015).

In the future, different activities can be pursued to shed light on the topic of the escape fraction of high-z galaxies and their relation with the reionization of the Universe. In particular, we are looking for possible faint ionizing galaxy populations combining high spatial resolution HST images from the CANDELS survey in GOODS-North with deep LBC imaging in the U-band (Grazian et al., in prep.) to measure the ionizing escape fraction at $z \sim 3$ in galaxies (and AGNs) fainter than those included in the present VUDS-LBC COSMOS field (i.e. $R \geq 25.5$). At relatively bright luminosities, the present sample can be significantly enlarged by the other two fields of the VUDS survey, i.e. the VVDS-02h region and the ECDFS, which benefit from relatively deep UV images by CFHT, Subaru, and the VLT (Le Fèvre et al. 2015; Vanzella et al. 2010b), respectively. Intrinsically faint galaxies ($L \ll L^*$) instead could be detected in LyC thanks to the large magnifications by strong lensing, as proposed by Vanzella et al. (2012b) and already carried out by Amorin et al. (2014). The cluster lensing and supernova survey with *Hubble* (CLASH, Postman et al. 2012) and the Frontier Field Initiative by HST will provide a large sample of highly magnified galaxies at high-z, which will open a new window onto the reionization process.

Acknowledgements. We thank the anonymous referee for her/his useful suggestions and comments that help us to improve this paper. We acknowledge financial contribution from the agreement ASI-INAF I/009/10/0. The LBT is an international collaboration among institutions in the United States, Italy, and Germany. LBT Corporation partners are The University of Arizona on behalf of the Arizona university system; Istituto Nazionale di Astrofisica, Italy; LBT Beteiligungsgesellschaft, Germany, representing the Max-Planck Society, the Astrophysical Institute Potsdam, and Heidelberg University; The Ohio State University; and The Research Corporation, on behalf of The University of Notre Dame, University of Minnesota, and University of Virginia. This work is supported by funding from the European Research Council Advanced Grant ERC-2010-AdG-268107-EARLY and by INAF Grants PRIN 2010, PRIN 2012 and PICS 2013. A.C., O.C., M.T. and V.S. acknowledge the grant MIUR PRIN 2010–2011. D.M. gratefully acknowledges LAM hospitality during the initial phases of the project. This work is based on data products made available at the CESAM data center, Laboratoire d'Astrophysique de Marseille. This work partly uses observations obtained with MegaPrime/MegaCam, a joint project of CFHT and CEA/DAPNIA, at the Canada-France-Hawaii Telescope (CFHT) which is operated by the National Research Council (NRC) of Canada, the Institut National des Sciences de l'Univers of the Centre National de la Recherche Scientifique (CNRS) of France, and the University of Hawaii. This work is based in part on data products produced at TERAPIX and the Canadian Astronomy Data Centre as part of the Canada-France-Hawaii Telescope Legacy Survey, a collaborative project of NRC and CNRS. Based on observations made with ESO Telescopes at the La Silla or Paranal Observatories under programme ID 175.A-0839. A.G. and E.V. warmly thank A. K. Inoue for providing the updated IGM transmission used in this paper. A.F. and J.S.D. acknowledge the contribution of the EC FP7 SPACE project ASTRODEEP (Ref. No: 312725).

References

Alavi, A., Siana, B., Richard, J., et al. 2014, ApJ, 780, 143
Alvarez, M. A., Finlator, K., & Trenti M. 2012, ApJ, 759, L38
Amorín, R., Grazian, A., Castellano, M., et al. 2014, ApJ, 788, L4
Becker, G. D., & Bolton, J. S. 2013, MNRAS, 436, 1023
Belotsky, K. M., & Kirillov, A. A. 2015, JCAP, 01, 041
Bertin, E., & Arnouts, S. 1996, A&AS, 117, 393
Bolton, J. S., Haehnelt, M. G., Viel, M., & Springel, V. 2005, MNRAS, 357, 1178
Boutsia, K., Grazian, A., Giallongo, E., et al. 2011, ApJ, 736, 41
Boutsia, K., Grazian, A., Giallongo, E., et al. 2014, A&A, 563, A142
Bouwens, R. J., Illingworth, G. D., Blakeslee, J. P., et al. 2004, ApJ, 611, L1
Bouwens, R. J., Illingworth, G. D., Oesch, P. A., et al. 2015a, ApJ, 803, 34
Bouwens, R. J., Illingworth, G. D., Oesch, P. A., et al. 2015b, ApJ, 811, 140
Bridge, C. R., Teplitz, H. I., Siana, B., et al. 2010, ApJ, 720, 465
Bruzual, A. G., & Charlot, S. 2003, MNRAS, 344, 1000
Calverley, A. P., Becker, G. D., Haehnelt, M. G., & Bolton, J. S. 2011, MNRAS, 412, 2543
Calzetti, D., Armus, L., Bohlin, R. C., et al. 2000, ApJ, 533, 682
Cassata, P., Le Fèvre, O., Garilli, B., et al. 2011, A&A, 525, A143
Cen, R., & Kimm, T. 2015, ApJ, 801, L25
Cooke, J., Ryan-Weber, E. V., Garel, T., & Diaz, C. G. 2014, MNRAS, 441, 837
Cowie, L. L., Barger, A. J., & Trouille, L. 2009, ApJ, 692, 1476
Cucciati, O., Tresse, L., Ilbert, O., et al. 2012, A&A, 539, A31
De Santis, C., Grazian, A., Fontana, A., & Santini, P. 2007, New Astron., 12, 271
Duncan, K., & Conselice, C. J. 2015, MNRAS, 451, 2030
Fan, X., Strauss, M. A., Becker, R. H., et al. 2006, AJ, 132, 117
Faucher-Giguère, C. A., Lidz, A., Hernquist, L., & Zaldarriaga, M. 2008, ApJ, 688, 85
Faucher-Giguère, C. A., Lidz, A., Zaldarriaga, M., & Hernquist, L. 2009, ApJ, 703, 1416
Finkelstein, S. L., Ryan, R. E. Jr., Papovich, C., et al. 2015, ApJ, 810, 71
Fiore, F., Puccetti, S., Grazian, A., et al. 2012, A&A, 537, A16
Fontanot, F., Cristiani, S., Pfrommer, C., Cupani, G., & Vanzella, E. 2014, MNRAS, 438, 2097
Giallongo, E., Cristiani, S., DOdorico, S., & Fontana, A. 2002, ApJ, 568, L9
Giallongo, E., Ragazzoni, R., Grazian, A., et al. 2008, A&A, 482, 349
Giallongo, E., Menci, N., Fiore, F., et al. 2012, ApJ, 755, 124
Giallongo, E. Grazian, A., Fiore, F., et al. 2015, A&A, 578, A83
Glikman, E., Djorgovski, S. G., Stern, D., et al. 2011, ApJ, 728, L26
Gnedin, N. Y., Kravtsov, A. V., & Chen, H.-W. 2008, ApJ, 672, 765
Grimes, J. P., Heckman, T., Aloisi, A., et al. 2009, ApJS, 181, 272
Grogin, N. A., Kocevski, D. D., Faber, S. M., et al. 2011, ApJS, 197, 35
Haardt, F., & Madau, P. 2012, ApJ, 746, 125
Hinshaw, G., Larson, D., Komatsu, E., et.al. 2013, ApJS, 208, 19
Ilbert, O., McCracken, H. J., Le Fèvre, O., et al. 2013, A&A, 556, A55
Inoue, A. K., & Iwata, I. 2008, MNRAS, 387, 1681
Inoue, A. K., Shimizu, I., Iwata, I., & Tanaka, M. 2014, MNRAS, 442, 1805
Iwata, I., Inoue, A. K., Matsuda, Y., et al. 2009, ApJ, 692, 1287
Ji-Hoon, K., Krumholz, M. R., Wise, J. H., et al. 2013, ApJ, 775, 109
Kimm, T., & Cen, R. 2014, ApJ, 788, 121
Kirkman, D., Tytler, D., Suzuki, N., et al. 2005, MNRAS, 360, 1373
Koekemoer, A. M., Faber, S. M., Ferguson, H. C., et al. 2011, ApJS, 197, 36
Kuhlen, M., & Faucher-Giguère, C.-A. 2012, MNRAS, 423, 862
Le Fèvre, O., Cassata, P., Cucciati, O., et al. 2013, A&A, 559, A14
Le Fèvre, O., Tasca, L. A. M., Cassata, P., & the VUDS Team 2015, A&A, 576, A79
Leitet, E., Bergvall, N., Hayes, M., Linné, S., & Zackrisson, E. 2013, A&A, 553, A106

Lilly, S. J., Le Fèvre, O., Renzini, A., et al. 2007, ApJS, 172, 70
Lusso, E., Worseck, G., Hennawi, J. F., et al. 2015, MNRAS, 449, 4204
Ma, X., Kasen, D., Hopkins, P. H., et al. 2015, MNRAS, 453, 960
Madau, P. 1995, ApJ, 441, 18
McLeod D. J., McLure, R. J., Dunlop, J. S., et al. 2015, MNRAS, 450, 3032
Meiksin, A. 2009, Rev. Mod. Phys., 81, 1405
Moller, P., & Jakobsen, P. 1990, A&A, 228, 299
Mostardi, R. E., Shapley, A. E., Nestor, D. B., et al. 2013, ApJ, 779, 65
Mostardi, R. E., Shapley, A. E., Steidel, C. C., et al. 2015, ApJ, 810, 107
Muzzin, A., Marchesini, D., Stefanon, M., et al. 2013, ApJ, 777, 18
Nestor, D. B., Shapley, A. E., Steidel, C. C., & Siana, B. 2011, ApJ, 736, 18
Nestor, D. B., Shapley, A. E., Kornei, K. A., Steidel, C. C., & Siana, B. 2013, ApJ, 765, 47
Paardekooper, J.-P., Khochfar, S., & Dalla Vecchia, C. 2013, MNRAS, 429, L94
Paardekooper, J.-P., Khochfar, S., & Dalla Vecchia, C. 2015, MNRAS, 451, 2544
Parsa, S., Dunlop, J. S., McLure, R. J., & Mortlock, A. 2015, MNRAS, submitted [arXiv:1507.05629]
Planck Collaboration XIII. 2015, A&A, submitted [arXiv:1502.01589]
Postman, M., Coe, D., Benitez, N., et al. 2012, ApJS, 199, 25
Prochaska, J. X., Worseck, G., & O'Meara, J. M. 2009, ApJ, 705, L113
Radovich, M., Arnaboldi, M., Ripepi, V., et al. 2004, A&A, 417, 51
Razoumov, A. O., & Sommer-Larsen, J. 2010, ApJ, 710, 1239
Reddy, N. A., & Steidel, C. C. 2009, ApJ, 692, 778
Roy, A., Nath, B. B., & Sharma, P. 2015, MNRAS, 451, 1939
Sawiki, M., & Thompson, D. 2006, ApJ, 642, 653
Scoville, N., Aussel, H., Brusa, M., et al. 2007, ApJS, 172, 1
Siana, B., Teplitz, H. I., Colbert, J., et al. 2007, ApJ, 668, 62
Siana, B., Teplitz, H. I., Ferguson, H. C., et al. 2010, ApJ, 723, 241
Siana, B., Shapley, A. E., Kulas, K. R., et al. 2015, ApJ, 804, 17
Shapley, A. E., Steidel, C. C., Pettini, M., Adelberger, K. L., & Erb, D. K. 2006, ApJ, 651, 688
Steidel, C. C., Pettini, M., & Adelberger, K. L. 2001, ApJ, 546, 665
Stevans, M. L., Shull, J. M., Danforth, C. W., & Tilton, E. M. 2014, ApJ, 794, 75
Stark, D. P., Walth, G., Charlot, S., Clement, B., & Feltre, A. 2015, MNRAS, submitted [arXiv:1504.06881]
Thomas, R., Le Fèvre, O., Cassata, P., et al. 2015, A&A, submitted [arXiv:1411.5692]
Topping, M. W., & Shull, J. M. 2015, ApJ, 800, 97
Tueros, M., del Valle, M. V., & Romero, G. E. 2014, A&A, 570, L3
Vanzella, E., Siana, B., Cristiani, S., & Nonino, M. 2010a, MNRAS, 404, 1672
Vanzella, E., Giavalisco, M., Inoue, A. K., et al. 2010b, ApJ, 725, 1011
Vanzella, E., Guo, Y., Giavalisco, M., et al. 2012a, ApJ, 751, 70
Vanzella, E., Nonino, M., Cristiani, S., et al. 2012b, MNRAS, 424, L54
Vanzella, E., de Barros, S., Castellano, M., et al. 2015, A&A, 576, A116
Wise, J. H., Demchenko, V. G., Halicek, M. T., et al. 2014, MNRAS, 442, 2560
Worseck, G., Prochaska, J. X., O'Meara, J. M., Becker, G. D., et al. 2014a, MNRAS, 445, 1745
Worseck, G., Prochaska, J. X., Hennawi, J. F., & Mcquinn, M. 2014b, ApJ, submitted [arXiv:1405.7405]
Wyithe, J. S. B., & Bolton, J. S. 2011, MNRAS, 412, 1926
Yajima, H., Li, Y., Zhu, Q., et al. 2014, MNRAS, 440, 776
Zahn, O., Reichardt, C. L., Shaw, L., et al. 2012, ApJ, 756, 65

[1] INAF–Osservatorio Astronomico di Roma, via Frascati 33, 00040 Monte Porzio Catone, Italy
e-mail: andrea.grazian@oa-roma.inaf.it
[2] Dipartimento di Fisica, Universitá di Roma La Sapienza, P.le A. Moro 2, 00185 Roma, Italy
[3] Aix-Marseille Université, CNRS, LAM (Laboratoire d'Astrophysique de Marseille) UMR 7326, 13388 Marseille, France
[4] INAF–Osservatorio Astronomico di Bologna, via Ranzani,1, 40127 Bologna, Italy
[5] Instituto de Fisica y Astronomía, Facultad de Ciencias, Universidad de Valparaíso, Av. Gran Bretaña 1111, Playa Ancha, Valparaíso, Chile
[6] INAF–IASF, via Bassini 15, 20133 Milano, Italy
[7] University of Bologna, Department of Physics and Astronomy (DIFA), V.le Berti Pichat, 6/2 - 40127 Bologna, Italy
[8] Astronomy Department, University of Massachusetts, Amherst, MA 01003, USA
[9] Department of Astronomy, University of Geneva, Ch. d'Écogia 16, 1290 Versoix, Switzerland
[10] Geneva Observatory, University of Geneva, Ch. des Maillettes 51, 1290 Versoix, Switzerland
[11] Institut de Recherche en Astrophysique et Planétologie – IRAP, CNRS, Université de Toulouse, UPS-OMP, 14 avenue E. Belin, 31400 Toulouse, France
[12] Department of Astronomy, California Institute of Technology, 1200 E. California Blvd., Pasadena, CA 91125, USA
[13] Institut d'Astrophysique de Paris, UMR7095 CNRS, Université Pierre et Marie Curie, 98bis boulevard Arago, 75014 Paris, France
[14] SUPA, Institute for Astronomy, University of Edinburgh, Royal Observatory, Edinburgh, EH9 3HJ, UK
[15] Space Telescope Science Institute, 3700 San Martin Drive, Baltimore, MD 21218, USA
[16] Centro de Estudios de Física del Cosmos de Aragón, 44001 Teruel, Spain
[17] Research Center for Space and Cosmic Evolution, Ehime University, Bunkyo-cho 2-5, 790-8577 Matsuyama, Japan

Appendix A: Other examples of contamination by foreground galaxies

We show here the cutouts in the *U*- and *R*-bands of LBC and in the I814W band by HST of peculiar sources of the VUDS-LBC/COSMOS field. These sources, in the last two subsections of Table 1, have been detected in LyC, but there are evidences of contamination by foreground sources closely aligned with the $z \sim 3.3$ sources, as mainly discussed in Sect. 4. In particular, Fig. A.1 shows two objects with global $f_{\rm esc}^{\rm rel} \geq 100\%$ and Fig. A.2 shows the example of four galaxies with global $f_{\rm esc}^{\rm rel} < 100\%$. In all the six galaxies, however, the local escape fraction is in the range ~200–1000%, thus indicating contamination by foreground sources.

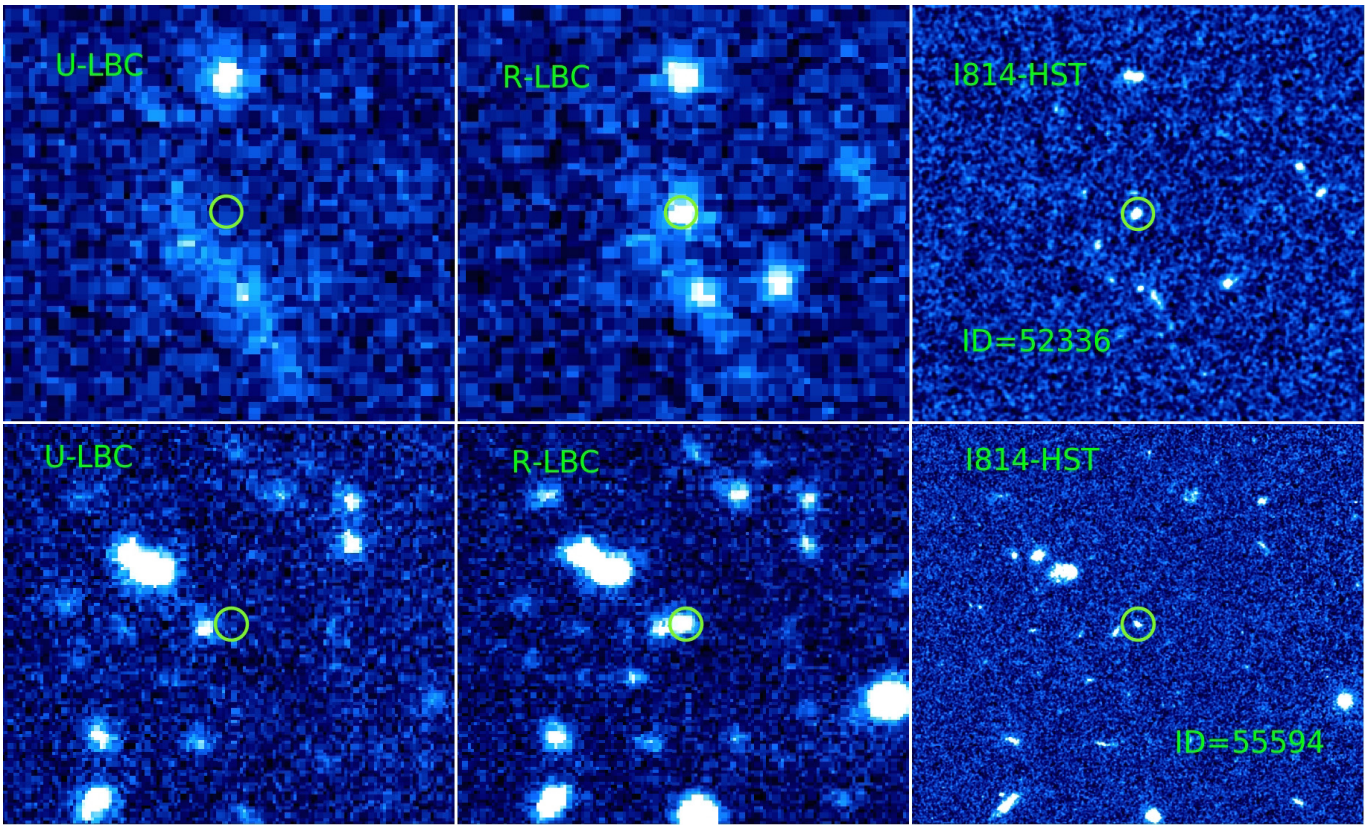

Fig. A.1. Cutouts of sources ID = 52336 and 55594 in the *U*-band (*left*) and in the *R*-band (*central panels*) by the LBC instrument. The *right* cutouts show the same sky area observed by HST in the *I814W* filter. The positions of the galaxies with spectroscopic redshifts $z \sim 3.3$ are indicated with green circles. The size of the cutouts is 12 arcsec for source ID = 52336 and 25 arcsec for ID = 55594, respectively.

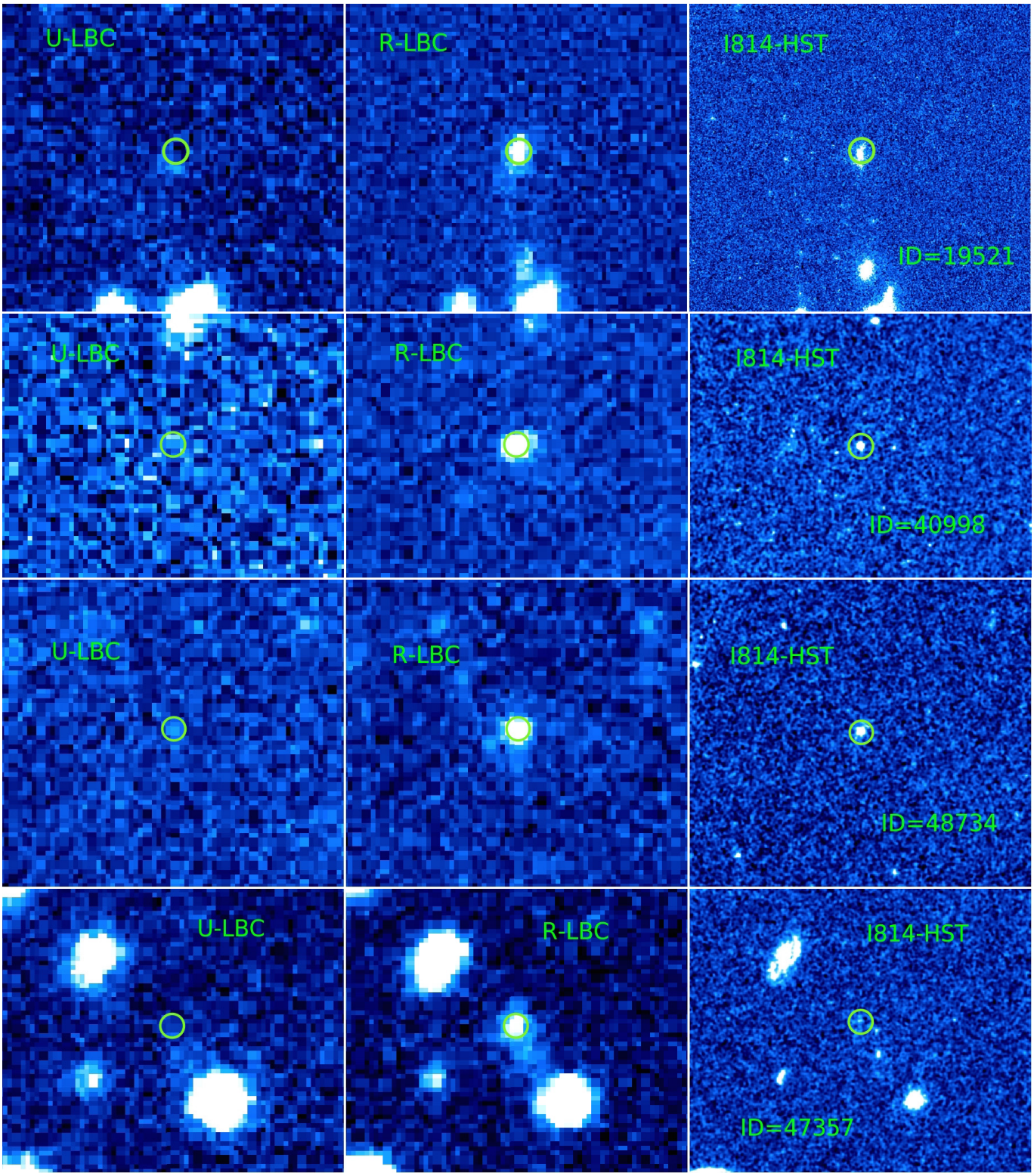

Fig. A.2. Cutouts of sources ID = 19521, 40998, 48734, and 47357 in the *U*-band (*left*) and in the *R*-band (*central panels*) by the LBC instrument. The *right* cutouts show the same sky area observed by HST in the *I814W* filter. The positions of the galaxies with spectroscopic redshifts $z \sim 3.3$ are indicated with green circles. The size of the cutouts is 15, 10, 12, and 10 arcsec for source ID = 19521, 40998, 48734, and 47357, respectively.